치의과학 박사학위논문

3D Printed Implants for Maxillofacial Reconstruction

악안면 재건을 위한 3D 프린팅 매식체

2019 년 2 월

서울대학교 대학원

치의과학과 구강악안면외과학 전공

이 의 룡

Abstract

3D Printed Implants for Maxillofacial Reconstruction

Part I. Osseointegration of titanium 3D printed implants with various structures

Part II. Impact of bioprinting on titanium 3D printed porous scaffold in periodontal ligament regeneration

Ui-Lyong Lee, DDS, MSD

Program in Oral and Maxillofacial Surgery, Department of Dental Science, Graduate School, Seoul National University

(Directed by Professor Pill-Hoon Choung, DDS, MSD, PhD)

Background and purpose of study

Maxillofacial area is not only responsible for the functioning of mastication for survival, but also important parts of social

functions such as language and appearance. Functional and aesthetic reconstruction is needed when a defect occurs caused by trauma, congenital anomaly, benign or malignant tumor. Although transplantation from other parts of the body has been successfully used for reconstruction of the maxillofacial area, there are various problems such as difficult operation, donor site morbidity, and non-esthetic results. In order to overcome this, a method of making patient-specific 3D printing titanium implants is being performed mainly in Europe and the United States. In Korea, patient-customized 3D printing titanium implants have been approved by Korean Food and Drug Association. However, researches on surface treatment and porous structure that can improve biocompatibility and osseointegration of 3D printed titanium implants are rare. Osseointegrated dental implants have been regarded as being very reliable and having long term predictability. However, host defense mechanisms against infection and micro-movement have been known to be impaired around a dental implant because of the lack of a periodontal ligament. To solve the problem, 3D printed hybrid artificial organ was fabricated by combining titanium 3D printing technology and bioprinting of periodontal ligament in this study.

The purpose of this study is to establish a mechanical and histological basis for the development of biocompatible maxillofacial reconstruction implant with osseointegration ability and to develop bio-implant resembling real tooth by fusing titanium 3D printed porous structure, microarc oxidation

and bioprinting technology.

Materials and Methods

Human periodontal ligament stem cells (hPDLSCs) and human bone marrow stem cells (hBMSCs) were obtained from extracted third molar. To characterize the immunophenotype of the hPDLSCs and hBMSCs, the expression of mesenchymal stem cell-associated surface markers was analyzed by flow cytometry. Next, the multi-lineage differentiation capacity of hBMSCs and hPDLSC were investigated *in vitro* with osteogenic, chondrogenic, and adipogenic medium. Titanium samples were fabricated by additive manufacturing and substractive manufacturing as disc-shaped. Manufactured disk-shaped samples were used either after treating surface by microarc oxidation (anodization) or not. To test the *in vitro* bioactivity of hBMSCs on various samples, hBMSCs adhesion assay, hBMSCs proliferation assay, and osteogenic differentiation marker analysis on 6 groups of samples were performed. Morphologic features of hBMSCs on various samples were observed by SEM. Specimens of the various porous structure produced by 3D printing titanium and solid structure produced by subtractive manufacturing with or without microarc oxidation were implanted in rabbit femurs. After 6 weeks, a push-out test, micro-CT, and histologic examination was performed to compare the degree of osseointegration and mechanical strength of each groups.

Various experiments were carried out to confirm that

bioprinting of human periodontal ligament stem cells is an effective method for regenerating periodontal ligament on 3D printed titanium. In this study bioink was mixture of a commercial 4% atelo-collagen, recombinant human fibroblast growth factor basic-2, and hPDLSCs with cell concentration in the bioink was $1x10^7$ cells/ml. hPDLSCs were seeded on the printed bioink without cells (group 1: titanium scaffold/collagen/cell seeding, group 2: titanium scaffold/collagen+FGF-2/cell seeding). In the cell printing group, the bioinks with cells (group 3: titanium scaffold/collagen/cell printing, group 4: titanium scaffold/collagen+FGF-2/cell printing) were printed one layer on a titanium scaffold surface and stored for 30 min at 37℃ for gelation

Morphologic features of seeded or printing hPDLSCs were observed by SEM. We cultured the samples till 21 days and took a photo every day to check the durability of gelled bioink. The viability and proliferation of seeded or printed hPDLSCs was evaluated by live/dead cell assay kit and CCK-8 solution. To evaluate gene expression levels of each samples, relative expression of ALP, Cemp1, and Col1 was evaluated with real-time PCR. Athymic rats were used for the animal experiment of transplantation of 3D printed titanium scaffold with seeded or cell printed hPDLSCs into a calvarial bone defect. Six weeks after transplantation, the rats were euthanized, and the calvaria with implanted specimens were harvested and histologic examination was done.

Results

SEM images verify that the total surface with micro-particles of anodized titanium 3D printed samples were coated with homogenous layer of nanoporous titanium oxides layer. hBMSCs adhesion assays demonstrated that nanopores on 3D printed titanium after anodization significantly outperformed samples with untreated surfaces. Anodized group showed significantly higher cell proliferation as compared to non-anodized groups at 14 days. At 7 days, cellular extensions were observed between micro-particles, and also entering into the nanopores that was shown on the surface of anodized samples. The most distinctive feature in osteogenic gene expression assay by RT-PCR is high OPG expression and low RANKL expression in anodized specimens. Push-out test showed that the 3D printed group was found to withstand a higher load than the subtractive manufacturing group. Microarc oxidation enhanced removal torque of 3D printed mesh implants. The titanium 3D printed solid samples showed better osseointegration than any other 3D printed mesh samples. Histologic examination showed that osseointegration was enhanced in the substractive manufactured group by anodization. Anodizing did not improve bone contact in 3D printed samples.

SEM showed that in the seeding groups (G1, G2) seeded hPDLSCs had no direction and were not well organized, but in the printing groups (G3, G4), printed hPDLSCs were well aligned and had direction. The gelled bioink did not collapse but remained in its originally printed form in all groups till 21 days.

Live/dead cell assay showed that in cell seeding, the cell distribution was uneven and cell aggregation was observed. In the cell printing group, the cell distribution was homogeneous and confirmed to consist of single cells without cell aggregation. In the CCK-8 assay, cell printing group proliferation has occurred well at day 7. At Day 7 of culture, the expression of CEMP1 in the cell printing group was significantly higher than in the cell seeding group. At 6 weeks after transplantation, the titanium 3D printed scaffolds were covered with fibrous connective tissue between the rat calvaria and scaffold in cell printing group. In undecalcified tissue specimen with H&E stain and basic fuchsin stain, new bone formation into porous scaffold was evident in seeding groups but in printing group, fibrous connective tissue was observed between the rat calvaria and scaffold. Immunohistochemical staining revealed that periostin, VWF, HLA, and CEMP1 were expressed in the tissues produced in the cell printing group.

Conclusion

The titanium 3D printed implant had better biocompatibility and osseointegration ability than the structure produced by conventional substractive manufacturing. Microarc oxidation enhanced removal torque of 3D printed mesh structure. But the 3D printed solid samples showed better osseointegration than any other 3D printed mesh structure. Therefore, the titanium 3D printed solid structure can be successfully used for maxillofacial reconstruction. Cell printing technology, rather than seeding periodontal ligament cells, has produced periostin

positive-connective tissue interface between titanium 3D printed scaffold and the bone. In this study, 3D printing hybrid implants resembling real tooth were developed by cell printing of periodontal ligament cells on the surface of titanium 3D printed implants, and the possibility of overcoming the limitation of conventional dental implants was demonstrated.

Keyword : stem cell, titanium 3D-printing, microarc oxidation, porous structure, bio-printing, biocompatibility, push-out test, osseointegration, 3D printed hybrid implant

Studuent Number : 2009-31124

Contents

Part I. Osseointegration of titanium 3D printed implants with various structures

Part II. Impact of bioprinting on titanium 3D printed porous scaffold in periodontal ligament regeneration

I. Introduction

II. Material and Methods

1. Primary cell culture from extracted human third molar

2. Flow cytometric analysis of the hPDLSCs

3. Osteogenic, chondrogenic, and adipogenic differentiation

4. Titanium 3D printed scaffold manufacturing for hPDLSCs printing

5. Preparation of hPDLSCs bioinks

6. Bioprinting process for periodontal ligament regeneration

7.Scanning Electron Microscopy (SEM) and sample observation

8. Live/dead cell assay and proliferation assay

9. Evaluation of the differentiation of seeded and printed hPDLSCs by real-time reverse transcription polymerase chain reaction (real-time PCR)

10. Animal experiments in athymic rat for evaluating PDL regeneration

Surgical Procedures

Histologic preparation for undecalcified sections

Part I. Osseointegration of titanium 3D printed implants with various structures

I. Introduction

Tumor resection, trauma, osteoradionecrosis, and various other causes may result in maxillofacial bone defects. The ultimate goal of reconstruction of maxillofacial bone defects is to restore bone defects and facial shape to its original form, minimize malocclusion, and restore masticatory function. In addition, the goal is to minimize the morbidity of donor and recipient and to perform reconstruction with minimum number of operations.[1, 2] There are many options for reconstruction of maxillofacial bone defects. Among them microvascular bone transfer have become the gold standard for reconstruction. But donor site morbidity, prolonged hospitalization time and a long recovery period with delayed functional rehabilitation are frequently noted.[3] Hence, there is increasing demand for alternatives of microvascular free osteocutaneous flap.[4]

Development of CAD-CAM technology and electron beam melting (EBM) with adequate strength and biocompatibility

makes the foundations for application of titanium patient-specific 3 dimensional printed implants in the field of maxillofacial bone reconstruction.[5-7] In fact, multicenter study about using patient-specific CAD/CAM reconstruction plates for mandibular reconstruction has been performed with good results,[8] while a case was reported on successful reconstruction of maxillomandibular defect using titanium 3D printed mesh.[4] EBM is a type of meal additive manufacturing method[9] in which a fine metal powder is melted in successive layers with a focused electron beam to manufacture a structure that may consist of various internal mesh structure and complex geometries.[10] Recent success in the manufacture of patient-specific 3D printed metal devices by additive manufacturing has been reported.[1, 4, 11] Such additive manufacturing method has benefits over existing titanium computerized control (CNC) milling method, as the internal configuration of the implant can be designed as desired. As the surface of implant can be fabricated with mesh structure, the increased porosity of the implant surface makes cell proliferation and mesenchymal stem cell differentiation improved and resulting in promotion of osseointegration.[5, 12, 13]

The essential point for successful reconstruction of maxillofacial bone defect with titanium 3D printed is

accomplishment of osseointegration.[14] The most important factor influencing the osseointegration of 3D printed titanium is macro mesh structures and nano surface properties.[15] Using CAD/CAM software various mesh type porous structures can be designed. Few studies have yet investigated which mesh structures should be used to best achieve osseointegration. In this study, various mesh type porous structures were designed and manufactured those using EBM. The degree of osseointegration was measured to find out the most beneficial mesh structure for osseointegration with animal experiment.

Porous structure of titanium implant can be manufactured using additive manufacturing technology but surface characteristics that affect tissue response can not be managed with 3D printing technology. Numerous surface treatment such as sandblasting, acid-etching, plasma reaction and electrochemical anodization have been utilized to improve the surface roughness.[16] Surface modification of titanium 3D printed implant should be performed to improve the osseointegration of implant in situation, such as reconstructing major-sized segmental mandibular defect of patients with osteoporosis.[14, 17, 18] If a segmental defect of the mandible is to be reconstructed, the reconstructed implant must withstand the masticatory force. Surface treatment of 3D printed porous structure is more

complicated than substractive manufactured solid implant because plasma spraying technique which widely used on solid implant can not be applied to porous structure.[14] Several surface modification methods for porous structure such as biomimetic coating, hydroxyapatite coating, heat treatment and chemical treatment have been reported. But there are many limitations that are not effective or time consuming in many cases.[17, 19–21] Recently microarc oxidation (anodization) which is an electrochemical technique was proposed for surface modification of 3D printed porous structure.[14, 22, 23] The biocompatibility and osteoconductivity/osteoinductivity of electrochemical treated surface are widely used in orthopedics and dental implant fixture.[24–27] Accordingly, we hypothesized that additive manufactured porous titanium implant with microarc oxidation could be utilized as reliable reconstructive implant for segmental maxillofacial bone defects. Bone formation around the 3D printed implant installed in rabbit femurs was evaluated and the mechanical strength of anodized 3D printed implants was measured with push out test.

II. Materials and Methods

1. Primary cell culture from extracted human third molar

Non-decayed human third molars that had been impacted in the mandible were extracted from 5 adults (18-28 years of age) under informed consent at the Seoul National University Dental Hospital, Seoul, South Korea. The experimental protocol was approved by the Institutional Review Board of the hospital (IRB No. 05004). During third molar extraction, bone marrow was obtained by curetting the extraction socket and the separated tissues were digested in a solution of 3 mg/mL collagenase type I (Worthington Biochem, Freehold, NJ) and 4 mg/mL dispase (Boehringer, Mannheim, Germany) for 1 h at 37C. Single-cell suspensions were collected by passing the cells through a 40-mm strainer (Falcon BD Labware, Franklin Lakes, NJ) and were cultured in the alpha-modification of Eagle's medium (alpha-MEM; Gibco BRL, Grand Island, NY) supplemented with 10% fetal bovine serum (Gibco BRL), 100 mM ascorbic acid 2-phosphate (Sigma-Aldrich, St. Louis, MO), 2mM glutamine, 100 U/mL penicillin, and 100 mg/mL streptomycin (Biofluids, Rockville, MD) and. The medium was changed after the first 24 h and then every 3 days. Three colonies of human bone marrow

stem cells (hBMSCs) were randomly picked and the cellular pool of those colonies was used for *in vitro* proliferation, differentiation studies, and animal experiment. All primary cells used in this study were in passage 2 or 3.

2. Flow cytometric analysis of the hBMSCs

To characterize the immunophenotype of the hBMSCs , the expression of mesenchymal stem cell-associated surface markers at passage 3 were analyzed by flow cytometry as previously reported.[32] hBMSCs in their third passage (1.0×10^6 cells) were fixed with 3.7% paraformaldehyde from 95% paraformaldehyde powder (Sigma-Aldrich) diluted in phosphate-buffered saline (PBS) (3.7 g/100 mL) for 10 min and re-suspended in PBS containing 1% bovine serum albumin (BSA) (ICN Biomedicals) for 30 min for blocking nonspecific antibody-binding sites. hBMSCs were then incubated with specific antibodies against CD34, CD13, CD90, or CD146 at 4° C for 1 h, and then incubated with fluorescent secondary antibodies at room temperature for 1 h. All used antibodies were purchased from BD Biosciences. The percentages of CD13-positive, CD90-positive, CD146-positive, and CD34-negative cells was measured using a FACS Calibur flow cytometer (Becton Dickinson Immunocytometry Systems). The

results were analyzed by CellQuest Pro software (Becton Dickinson).

3. Osteogenic, chondrogenic, and adipogenic differentiation of the hBMSCs

To promote osteogenic, chondrogenic, and adipogenic differentiation, hBMSCs were cultured in StemPro Osteogenic, StemPro Chondrogenic, and StemPro Adipogenic differentiation medium (Gibco BRL), respectively, with the appropriate supplements as previously reported.[32] At 21 days, the cells with post-osteogenic, post-chondrogenic, and post-adipogenic induction were stained with 2% Alizarin Red S stain at pH 4.2 (Sigma-Aldrich), 1% Alcian Blue (Sigma-Aldrich), and 0.3% Oil Red O dye (Sigma-Aldrich) to detect proteoglycans, Nissl bodies, and fat vacuoles as indicators of osteogenic, chondrogenic, and adipogenic differentiation, respectively. Stained cells were observed and those were visualized under an inverted light microscope (Olympus U-SPT; Olympus).

4. Manufacturing of titanium 3D printed samples for *in vitro* assay

Two CAD/CAM programs (3-Matic/MAGICS, Materialise, Belgium) were utilized to design a 3D printed samples for *in*

vitro assay. The porous structures were based on dode-thin unit cells in the MAGICS program with the following design (nominal) dimensions: strut size = 120 μm, pore size = 500 μm, porosity = 88%. Solid structure were also designed without any pores. The designed STL file was programmed to a 3D printer with an EBM method of metal additive manufacturing (Arcam A1, Arcam, Sweden), and samples were printed using Ti-6Al-4 V-ELI medical grade powder (Arcam A1, Arcam, Sweden). The composition of the Ti-6Al-4 V-ELI medical grade powder was 5.94% Al, 4.14% V, 0.008% C, 0.049% Fe, 0.10% O, 0.010% N, 0.010% Y, and less than 0.002% H and Z, with the remaining composition being Ti (in weight percent).[1] The powder was also purchased from Arcam and was designed specifically for additive manufacturing.

In this system, the focused high energy electron beam was rastered over each successive layer of Ti-6Al-4 V-ELI medical grade powder, which was gravity-fed from powder containers and raked into successive layers of approximately 50 μm in thickness. The building component was moved down on the build table with the finishing of each successive layer. Each newly raked powder layer was initially rastered by the electron beam after approximately 11 passes at a beam current of approximately 35 mA to preheat each layer to approximately

600 ° C. The melt configuration was determined by a three dimensional CAD program that melts only selected layer areas to add metal to the build.[1, 9] For subtractive manufacturing, Ti-6al-4V-ELI medical-grade material was used. Disk-shaped samples with various size (Ø14 mm xH2 mm, Ø18 mm x H2 mm) were manufactured with additive and substractive manufacturing for *in vitro* assays (Fig. 1).

5. Surface Treatments (Microarc oxidation)

Manufactured disk-shaped samples were ultrasonically cleaned in acetone, ethanol, and distilled water by sequentially for surface degreasing. The anodization treatment was performed on each of structures to form homogenized nanoporous structure. Nanoporous structures were fabricated by DC power supply (N8943A DC power supply, Keysight, California, US) at room temperature, treatment was applied voltage and current from 100 to 200 V with 1A until to be a passivation (zero current). The samples were used as an anodes while a platinum plate was worked as a cathode, aqueous electrolyte solution was 1.0 M H_3PO_4 which has prepared from reagent grade chemicals and distilled water. The surface morphology was observed by field emission scanning electron microscopy (FE-SEM, Ultra plus, Zeiss, Deutschland).

The phases of anodized surface of 3D printed samples were analyzed by energy disperse spectroscopy (S-4800, Hitachi, Japan).

6. Cell adhesion assay

Human BMSCs ($5x10^4$ cells/wells) were seeded onto 6 samples (Ø14 mm x H2 mm) and cultured for up to 3 hours in alpha-MEM (Welgene, Fresh Media, Korea) containing 10% FBS (Gibco, by life technologies, USA) and 1x Antibiotic (Gibco, by life technologies, USA) at 37 ° C in a humidified atmosphere containing 5% CO_2. Samples are relocated to a new plate, unattached cells were removed by vigorous pipetting with phosphate-buffered saline (PBS), and the remaining hBMSCs were measured. The quantitative analysis was carried out using a WST-8 assay (Viability Assay Kit, MediFab Co., LTD) at OD 450 nm.

7. Cell proliferation assay

Cell proliferation was analyzed using a WST-8 assay (Viability Assay Kit, MediFab Co., LTD). Human BMSCs ($5.0 x 10^4$ cells/well) were seeded in 6 samples (Ø14 mm x H2 mm) and cultured for 1, 7, 14 days. Samples with cultured hBMSCs were transferred to a new plate, washed with alpha MEM

medium and add the medium and Cellrix viability assay kit are mixed at a ratio of 5:1 to each well of the plate. Incubated the plate for 2 hours at 37 ° C in 5% CO_2. Then, Inoculated cell suspension (100㎕/well) in a 96-well plate and the absorbance at 450 nm using an ELISA reader was measured.

8. Osteogenic differentiation marker analysis by RT-PCR

To evaluate osteogenic gene expression levels, $5.0x10^4$ hBMSCs were seeded in 6 samples (Ø18 mm x H2 mm) (3 wells/each sample) and cultured for 7 days, 14 days and 21 days under osteogenic differentiation induction conditions as DMEM (Welgene, Fresh Media, Korea) containing 10% FBS, 1x Antibiotics, 10mM glycerol 2-phosphate, 50㎍/mL ascorbic acid and 1mM dexamethasone. Total RNA was harvested from the samples using Trizol reagent (Life Technologies, NY, USA) and cDNA was synthesized from 1 ㎍ of total RNA using reverse transcriptase (Superscript II Preamplification System; Invitrogen). The expression of the selected osteogenic genes ALP, Runx2, OPN, RANKL, OPG and OCN were quantified using SYBR green gene expression assays on Step One Plus PCR system (Applied Biosystems) according to manufacturer' s instructions. All reactions were run in triplicate and were normalized to the reference gene (GAPDH). The specific

primer sets used for this analysis are listed in Table 1.

9. Scanning Electron Microscopy (SEM)

Human BMSCs that adhered onto the 6 samples (Ø14 mm x H2 mm) surfaces were fixed with modified Karnovsky's fixative for 2 hours. The samples were washed 3 times with PBS buffer for 15 min and fixed with 1% osmium tetroxide (EMS). The samples were then washed with distilled water and dehydrated with graded concentrations (70, 80, 90, 95 and 100% v/v) of ethanol. The samples were then treated with hexamethyl disilazane (HMDS) for 20 min. Finally, the samples were coated with Pt prior to cell shape observation with field emission scanning electron microscope (FE-SEM; Hitachi S-4700) using an acceleration voltage of 15kV.

10. Animal experiments in rabbits

3D printed titanium implant preparation

This process was performed by ISO10993-6:2007 (tests for local effects after implantation, Annex D-Test method for implantation in bone).[9] 5 types of specimens (Ø2.5 mm x6.0 mm) were manufactured, 4 types (soild, dode-thin, octadense, and G-structure) by additive manufacturing and one sample manufactured by subtractive manufacturing (fig. 2). Half of the

specimens were anodized as previous described.

Implantation in rabbits

Ten male rabbits (New Zealand White) were purchased from Orient Bio Inc. New Zealand White rabbits (3200 g) were selected as they have already been widely used for implant tests[9, 29]. The study protocol was approved by the Ethics Committee on Animal Experimentation of Chung-Ang University (2019-00002). Before transplantation, fur was shaved around a portion of the rabbit femur to ensure there was enough space to implant test materials. After the rabbits were anesthetized with alfaxanolone (Alfaxan®,Jurox, Australia) (4mg/kg) and xylazine hydrochloride (Rompun®,Bayer Korea, Korea) (0.32 ml/kg) IM , implantation site of femur were approached with 7 cm long incisions through the skin. And all specimens were implanted in individual rabbits (Fig. 3). Six weeks after implantation, the rabbits were euthanized, and the femurs with implanted specimens were enucleated.

Push-out test to compare the degree of osseointegration

The enucleated portion was fixed to a jig, and the push-out test was performed (Instron 5966, Illinois Tool Works Inc., USA) in the same rod as specimen size (Ø 2.5 mm) (Fig. 4).

Micro-CT procedure

The femur area that included the implanted samples was harvested and subjected to micro-CT. Each sample was scanned with a Skycan-1173 Micro-CT (Bruker MicroCT, Kontich, Belgium) with the following parameters: 130 kV tube voltage, 60 μA current, 0.5 mm copper+aluminium filter, 14.91 μm image pixel size, 400 ms exposure time, 0.5° rotation step, 360° scan and 3 frames per rotation. Three-dimensional (3D) reconstructions were performed using NRecon software (Bruker MicroCT). 30 consecutive sections of each sample were placed on the cortical bone. The total length of each sample (TL) was measured at each cross section and the length of the portion in contact with the bone (BL) was measured to analyze the ratio of the portion in contact with the bone.

Histologic preparation for undecalcified sections

Specimens were dehydrated in a graded concentration of ethanol and embedded in methyl methacrylate resin (Technovit® 7200; Heraeus Kulzer, Wehrheim, Germany) as previously reported[29]. Blocks of methyl methacrylate including the samples were sectioned at 100-μm thickness in the sample's long axis using a diamond-coated saw cutter and the Exakt grinding system (EXAKT Advanced Technologies GmbH,

Norderstedt, Germany). And followed by the sections were further ground and polished to 20-μm thickness. The sections were then stained with basic fuchsin and methylene blue, by which the bone was stained red. The percentage of bone implant contact (BIC) was analyzed by image-analysis software (AxioVision 4.8; Carl-Zeiss MicroImaging GmbH, Gottingen, Germany).

11. Statistical analysis

Statistical analysis was performed by one-way analysis of variance (ANOVA) followed by Bonferroni's multiple comparison test using SPSS (ver.18) software for a comparison between the groups. $P < 0.05$ was used as the significance level.

III. Results

1. Characterization of hBMSCs

Human BMSCs from the mandibular third molars extraction socket were isolated and expanded. In order to characterize the hBMSCs, flow cytometric analysis was performed using mesenchymal stem cell markers including CD13, CD34, CD90, and CD146.[33] Flow cytometric analysis showed that approximately 91.39% of the hBMSCs expressed CD13, 93.63% expressed CD90, 55.71% expressed CD146, and 11.09% expressed CD34 (Fig. 5). CD34 is known as MSC-negative marker, which marks primitive endothelial cells and hematopoietic progenitors.[34]

Next, the multi-lineage differentiation capacity of hBMSCs was investigated *in vitro* with osteogenic, chondrogenic, and adipogenic medium. After 3 weeks of osteogenic and adipogenic induction, hBMSCs formed extensive Alizarin red S-positive mineral deposits and Oil Red O-positive lipid droplets throughout the adherent layers. Furthermore, hBMSCs also formed Alcian Blue-positive nodules after incubation in chondrogenic induction medium (Fig. 6).

2. Surface morphology of 3D printed titanium after

anodizing

The typical topography of samples with micro-particles morphology manufactures by 3D printing and revealed by SEM is presented in Figure 7. SEM images demonstrate that 3D printed samples' surface is entirely covered by globular micro-particles with different sizes arbitrarily disseminated on the surface. The rough and uneven surface morphology, ranging from about 20 μm to 50 μm for size of micro-particles, with a wide range of inter-particle distance was observed (Fig. 7A, 7B, 7C, and 7D).

The SEM images revealing nanopores on samples after the anodization process are demonstrated in Figure 7C, 7D, and 7E. SEM images verify that micro-particles remained the anodization process, and that the total surface with micro-particles of samples were coated with homogenous layer of nanoporous titanium oxides layer. The microarc oxidation seems to have little influence on macrostructure with micro-particles. The additive manufactured surface consisted of micro-particles and flat surface, which after microarc oxidation is coated with nanopores. The microarc oxidation was performed at 170 V for 20 min. After anodization, the all 6 samples loses its metallic luster and became dark (fig. 1). The

chemical constitution and state of the components in the 3D printed sample surface after microarc oxidation was characterized by energy disperse spectroscopy (EDS). According to the EDS, the main surface components are O, Ti, Al, and V (Fig. 8).

3. Human BMSCs attachment assay on various surfaces

Human BMSCs adhesion assays demonstrated that nanopores on 3D printed titanium after anodization significantly outperformed samples with untreated surfaces (Fig. 9). Cell adhesion efficacy was found to be: anodized 3D printed mesh titanium (A3DPMTi) > 3D printed mesh titanium (3DPMTi) > anodized 3D printed solid titanium (A3DPSTi) > 3D printed solid titanium (3DPSTi) > subtractive titanium (STi) = anodized subtractive titanium (ASTi). The cellular spread morphology seemed to correlate with the surface roughness with nanopores of the samples, with more rapid attachment and spread overall evident for the anodized 3D printed samples.

4. Human BMSCs proliferation assay on various surfaces

Human BMSCs showed a well proliferation in all groups (Fig.

10). The WST-8 assay of 1 day cultures identified no significant difference in the number of cells between the groups. Anodized group showed significantly higher cell proliferation as compared to non-anodized groups at 14 days (Fig. 10). Cell number analyzed by total DNA content was consistent with the observations based on metabolic activity. 3D printed samples had significantly higher DNA amounts as compared to substractive manufactured samples at 14 days (Fig. 10).

5. Morphologic features of hBMSCs (SEM)

The morphology of hBMSCs attached after 7 days of culture on the various samples by SEM is shown in Figure 11. At 7 days, cellular extensions were observed between micro-particles (Fig. 11), and also entering into the nanopores that was shown on the surface of anodized samples. Surface morphology of the anodized additive manufactured samples, with micro-scale micro-particles, in associated with nanoporous coating, produces a surface that enhances strong anchoring of the hBMSCs. The cellular morphology shown with SEM seemed to correlate with the result that hBMSCs adhesion assays showed that nanopores on 3D printed titanium after anodization significantly outperformed samples with untreated surfaces.

6. Osteogenic gene expression by RT-PCR

At Day 7 of culture, the expression of OCN in the non-anodized group was higher than in the anodized group. The relative expression of OPG was elevated in cells cultured on anodized samples (Fig. 12A). ALP, Runx2, RANKL, and OPG did not show any particular differences between both groups. After 14 days, the expression of ALP, OCN, and RANKL in the 3D printed non-anodized group was higher than in the anodized group. However anodized 3D printed mesh titanium (A3DPMT) exhibited greater expression of OPN as compared to non-anodized surfaces. The relative expression of OPG was elevated in cells cultured on anodized samples (Fig. 12B). At Day 21, the expression of the osteoclastogenic inhibitory factor OPG was elevated on anodized surfaces (Fig. 12C). Anodized surfaces also showed lowered expression of RANKL, OCN, and OPN (Fig. 12C).

7. Push-out test to compare the degree of osseointegration

As shown in Figure 13. the anodized group was found to withstand a higher load than the non-anodized group in 3D printed mesh group. And the 3D printed group was found to withstand a higher load than the subtractive manufacturing group. 3D printed solid group was found to withstand a highest

load about 260 N. As shown in Figure 13, the 3D printed solid samples showed better osseointegration than any other 3D printed mesh structure. Even though the solid specimens do not have porous structure, there were numerous spherical particles attached to the specimen as shown in the above SEM image, It is thought that it played a role of osseointegration. Anodization reduced removal torque significantly in 3D printed solid group. Among 5 groups, structures that statistically significant increases in maximum load was dode-thin by anodization (Fig. 13).

8. Micro-CT analysis for analyzing the ratio of the portion in contact with the bone.

After 6 weeks of healing, all implants were in close contact with the surrounding bone except subtractive titanium (STi) (Fig. 14). New woven bone was observed on the implant surfaces. The bone around the anodized subtractive manufactured implant was apparent, confirming that bone formation had almost occurred but poor bone implant contact (BIC) was observed in the non-anodized subtractive manufactured implant (STi) (Fig.14A). The anodized and non-anodized 3D printed structure (3DPSTi, 3DPM1Ti, 3DPM2Ti, and 3DPM3Ti) produced by additive manufacturing showed

confirmation that bone formation around implant was very well (Fig. 14B-E). The total length of each sample (TL) was measured at each cross section and the length of the portion in contact with the bone (BL) was measured to analyze the ratio of the portion in contact with the bone. The BL/TL of the cortical femur bone in the Sti (49.9 %) was lowest value and in the 3DPSTi (92.5 %) was the highest value. Micro-CT analysis did not show any particular differences between non-anodized and anodized groups (Fig. 15).

9. Histologic analysis for evaluation bone implant contact

Histologic examination obtained in the cortical region of each group implants which implanted in rabbit's femur at 6 weeks are presented in Figures 16, 17, 18, 19, and 20. In the peri-implant cortical region, the STi (Fig. 16), 3DPSTi (Fig. 17), 3DPM1Ti (dode-thin) (Fig. 18), 3DPM2Ti (G-structure) (Fig. 19), and 3DPM3Ti (Octadens) (Fig. 20) implants were osseointegrated and demonstrated multiple areas of contact between the femur bone and the implant surface except substractive manufactured sample without anodization.

IV. Discussion

The purpose of this study is to establish a mechanical and histological basis for the development of biocompatible maxillofacial reconstruction implants by fusing titanium 3D printed porous structure and surface treatment. Improved osseointegration of titanium 3D printed implant for maxillofacial segmental bone defect reconstruction could be advantageous in not only quickly osseointegrated to the bone tissue but also stabilizing the reconstruction. Rigid stability of reconstruction would provide favorable environment for bone healing even in critical-sized bone defect of immediately loaded site like mandible or maxilla.[35] But the main manufacturing method currently utilized in the medical manufacturing industry is to cut or trim a large raw material (subtractive manufacturing).[9] The FDA-approved patient-specific TMJ prosthesis (TMJ Concept®) is also produced in subtractive manufacturing. This study established the mechanical and histologic background for the 3D printed implant with various mesh structure and surface treatment for maxillofacial reconstruction. In this study, we implanted in rabbit femurs specimens of the various porous structure produced by titanium 3D printing with metal powder and solid structure produced by subtractive manufacturing with

or without microarc oxidation. After 6 weeks, a push-out test was performed to compare the degree of osseointegration and mechanical strength of each groups.

Currently, virtual surgical planning using the software and additive manufacturing technology provides a valuable tool to support accurate surgical planning and precise surgery in maxillofacial reconstruction.[1] Multicenter study on the use of patient-specific CAD/CAM reconstruction plates for mandibular reconstruction showed that mandibular reconstruction using patient-specific mandible reconstruction plates (PSMPs) offers a broad range of opportunities and benefits compared with standard procedures.[8] The use of CAD/CAM technology for the fabrication of surgical resection guides and mandibular reconstruction plates has proven to be useful for accurate surgical result.[36] Matthew et al. reported CAD and rapid prototype modelling have the potential to increase the speed and accuracy of mandibular reconstruction.[37]

Various reconstructive options are possible for maxillofacial bone defects. Recently microvascular bone grafts have become the method of choice for facial bone reconstruction to restore the aesthetic and functional aspects of the upper and lower jaw. But these extended operations are not appropriate for some patients. Donor site morbidity, increased risk of recurrence due

to delayed radiotherapy, prolonged hospitalization time with increased cost and a long recovery process with delayed function are frequently noted disadvantages.[3] Also, with increasing life expectancy, there are increasing cases of maxillomandibular reconstructions in elderly with multiple medical problems, where long reconstructive surgical procedure would be unsuitable. Hence, there is increasing demand for finding alternatives to the gold standard procedures of maxillomandibular reconstructions by microvascular free osteocutaneous flap.

Recent success in the fabrication of patient specific titanium biomedical devices by additive manufacturing has been reported.[1, 4, 11] Such EBM method has advantages over existing titanium computerized control (CNC) milling method of CAD/CAM technology, as the internal structure of the implant can be freely designed. As the surface architecture can be controlled freely using the computer aided design, the porosity of the portion that would be in contact with bone can be increased, resulting in promotion of bone–implant anchorage by improving cell proliferation and mesenchymal stem cell differentiation.[5, 12, 13] Indeed, further investigations on various designs, mesh structures and surface treatment of samples produced by additive manufacturing would be required.

Expanded hBMSCs from the human extraction socket were used for *in vitro* test. Stemness of hBMSCs from extraction socket was shown in this study. Human BMSCs were used in our experiments because the maxillofacial reconstruction implants are actually contacting and interacting these cells.

Appropriate surface roughness of implants enhances osteoblastic functions, including adhesion, proliferation and differentiation, which are considered to be the vital requirements in order to achieve successful osseointegration.[38] Previous reports have shown that titanium implants with micro-scale associated with nano-scale promote osteoblastic cell functions.[39] Accordingly, we hypothesized that additive manufactured titanium implant could be used as reliable reconstructive materials for immediately loaded segmental maxillofacial bone defects by anodizing. There is no difference between solid and mesh specimens when observed at high magnification

SEM images demonstrate that 3D printed samples' surface is entirely covered by globular micro-particles with different sizes arbitrarily disseminated on the surface. The SEM images revealing nanopores on samples after the anodization process are demonstrated in Figure 7C,7D, and 7E. SEM images verify that micro-particles remained the anodization process, and that

the total surface with micro-particles of samples were coated with homogenous layer of nanoporous titanium oxides layer. The chemical constitution and state of the components in the 3D printed sample surface after microarc oxidation was characterized by energy disperse spectroscopy (EDS). According to the EDS, the main surface components are O, Ti, Al, and V. During microarc oxidation aqueous electrolyte solution (1.0 M H_3PO_4) was used. Remaining H_3PO_4 on implant surface can be cytotoxic. We confirmed that there was no phosphate on samples using EDS.

Human BMSCs adhesion assays demonstrated that nanopores on 3D printed titanium after anodization significantly outperformed samples with untreated surfaces. The cellular morphology shown wit SEM seemed to correlate with the result that hBMSCs adhesion assays showed that nanopores on 3D printed titanium after anodization significantly outperformed samples with untreated surfaces. Anodized group showed significantly higher cell proliferation as compared to non-anodized groups at 14 days. Previous studies have shown that cells are likely to elongate or stretch on nanoporous surfaces.[38]

At Day 7 of culture, the relative expression of OPG was elevated in cells cultured on anodized samples (Fig. 12A). After 14 days, the expression of ALP, OCN, and RANKL in the 3D

printed non-anodized group was higher than in the anodized group. The relative expression of OPG was elevated in cells cultured on anodized samples (Fig. 12B). At Day 21, the expression of the osteoclastogenic inhibitory factor OPG was elevated on anodized surfaces (Fig. 12C). Anodized surfaces also showed lowered expression of RANKL, OCN, and OPN (Fig. 12C). The most distinctive feature in osteogenic gene expression assay is high OPG expression and low RANKL expression in anodized specimens. Consequently anodization may have the effect of inhibiting osteoclastogenesis like bisphosphonate. RANKL (receptor activator of NF-κB ligand), a membrane-bound molecule, is a newly established member of the tumor necrosis factor (TNF) ligand family and has been known as essential for osteoclast formation.[40] And osteoprotegerin (OPG), a member of the tumor necrosis factor receptor (TNF-R) superfamily[41, 42] acts as a decoy receptor by inhibiting the interaction of RANKL with its functional receptor RANK[43], consequently blocking osteoclastogenesis. Many studies have reported that widely used osteoclast inhibitors, the bisphosphonate, promote osseointegration.[44] 3D printed solid group was found to withstand a highest load about 260 N. As shown in Figure 13, the 3D printed solid samples showed better osseointegration than any other 3D printed mesh structure.

Even though the solid specimens do not have porous structure, there were numerous spherical particles attached to the specimen as shown in the above SEM image, It is thought that it played a role of osseointergration. After 6 weeks of healing, all implants were in close contact with the surrounding bone except subtractive titanium (STi) (Fig. 14). New woven bone was observed on the implant surfaces. Anodizing did not improve bone contact in mesh structure implants. Few studies have investigated impact of microarc oxidation on 3D printing mesh structures. Xiu et al. concluded that surface treatment of 3D printed mesh structure with microarc oxidation improved bone-in- growth capacity and bone bonding to implant surface.[14] Microarc oxidation should be performed under various conditions to find the best tissue reaction in further study.

V. Conclusion

Titanium 3D printed structures were found to withstand a higher load than the conventional titanium subtractive manufacturing samples. Based on the results of this study titanium 3D printed solid structure can be used for maxillofacial reconstruction with good results respect to osseointegration and bone healing, with a statistically significantly higher removal loading compared to substractive manufactured group and 3D printed mesh groups with or without anodization.

References

1. Lee UL, Kwon JS, Woo SH, Choi YJ. Simultaneous Bimaxillary Surgery and Mandibular Reconstruction With a 3-Dimensional Printed Titanium Implant Fabricated by Electron Beam Melting: A Preliminary Mechanical Testing of the Printed Mandible. *J Oral Maxillofac Surg*. 2016; 74: 1501 e1501-1501 e1515.
2. Lee DJ, Lee JM, Kim EJ, Takata T, Abiko Y, Okano T *et al.* Bio-implant as a novel restoration for tooth loss. *Sci Rep*. 2017; 7: 7414.
3. Ettl T, Driemel O, Dresp BV, Reichert TE, Reuther J, Pistner H. Feasibility of alloplastic mandibular reconstruction in patients following removal of oral squamous cell carcinoma. *J Craniomaxillofac Surg*. 2010; 38: 350-354.
4. Shan XF, Chen HM, Liang J, Huang JW, Cai ZG. Surgical Reconstruction of Maxillary and Mandibular Defects Using a Printed Titanium Mesh. *J Oral Maxillofac Surg*. 2015; 73: 1437 e1431-1439.
5. Bertollo N, Da Assuncao R, Hancock NJ, Lau A, Walsh WR. Influence of electron beam melting manufactured implants on ingrowth and shear strength in an ovine model. *J Arthroplasty*. 2012; 27: 1429-1436.

6. Hrabe NW, Heinl P, Flinn B, Korner C, Bordia RK. Compression-compression fatigue of selective electron beam melted cellular titanium (Ti-6Al-4V). *J Biomed Mater Res B Appl Biomater*. 2011; 99: 313-320.

7. Joshi GV, Duan Y, Neidigh J, Koike M, Chahine G, Kovacevic R *et al.* Fatigue testing of electron beam-melted Ti-6Al-4V ELI alloy for dental implants. *J Biomed Mater Res B Appl Biomater*. 2013; 101: 124-130.

8. Wilde F, Hanken H, Probst F, Schramm A, Heiland M, Cornelius CP. Multicenter study on the use of patient-specific CAD/CAM reconstruction plates for mandibular reconstruction. *Int J Comput Assist Radiol Surg*. 2015; 10: 2035-2051.

9. Lim JY, Kim N, Park JC, Yoo SK, Shin DA, Shim KW. Exploring for the optimal structural design for the 3D-printing technology for cranial reconstruction: a biomechanical and histological study comparison of solid vs. porous structure. *Childs Nerv Syst*. 2017; 33: 1553-1562.

10. Murr LE, Gaytan SM, Martinez E, Medina F, Wicker RB. Next generation orthopaedic implants by additive manufacturing using electron beam melting. *Int J*

Biomater. 2012; 2012: 245727.

11. Watson J, Hatamleh M, Alwahadni A, Srinivasan D. Correction of facial and mandibular asymmetry using a computer aided design/computer aided manufacturing prefabricated titanium implant. *J Craniofac Surg*. 2014; 25: 1099–1101.
12. Lv J, Xiu P, Tan J, Jia Z, Cai H, Liu Z. Enhanced angiogenesis and osteogenesis in critical bone defects by the controlled release of BMP–2 and VEGF: implantation of electron beam melting–fabricated porous Ti6Al4V scaffolds incorporating growth factor–doped fibrin glue. *Biomed Mater*. 2015; 10: 035013.
13. Yang J, Cai H, Lv J, Zhang K, Leng H, Wang Z *et al.* Biomechanical and histological evaluation of roughened surface titanium screws fabricated by electron beam melting. *PLoS One*. 2014; 9: e96179.
14. Xiu P, Jia Z, Lv J, Yin C, Cheng Y, Zhang K *et al.* Tailored Surface Treatment of 3D Printed Porous Ti6Al4V by Microarc Oxidation for Enhanced Osseointegration via Optimized Bone In–Growth Patterns and Interlocked Bone/Implant Interface. *ACS Appl Mater Interfaces*. 2016; 8: 17964–17975.
15. Hollister SJ. Scaffold design and manufacturing: from

concept to clinic. *Adv Mater*. 2009; 21: 3330-3342.

16. Losic D, Aw MS, Santos A, Gulati K, Bariana M. Titania nanotube arrays for local drug delivery: recent advances and perspectives. *Expert Opin Drug Deliv*. 2015; 12: 103-127.

17. Amin Yavari S, van der Stok J, Chai YC, Wauthle R, Tahmasebi Birgani Z, Habibovic P *et al.* Bone regeneration performance of surface-treated porous titanium. *Biomaterials*. 2014; 35: 6172-6181.

18. Lopez-Heredia MA, Sohier J, Gaillard C, Quillard S, Dorget M, Layrolle P. Rapid prototyped porous titanium coated with calcium phosphate as a scaffold for bone tissue engineering. *Biomaterials*. 2008; 29: 2608-2615.

19. Biemond JE, Hannink G, Verdonschot N, Buma P. Bone ingrowth potential of electron beam and selective laser melting produced trabecular-like implant surfaces with and without a biomimetic coating. *J Mater Sci Mater Med*. 2013; 24: 745-753.

20. Li X, Feng YF, Wang CT, Li GC, Lei W, Zhang ZY *et al.* Evaluation of biological properties of electron beam melted Ti6Al4V implant with biomimetic coating *in vitro* and in vivo. *PLoS One*. 2012; 7: e52049.

21. Mroz W, Budner B, Syroka R, Niedzielski K, Golanski G,

Slosarczyk A *et al.* In vivo implantation of porous titanium alloy implants coated with magnesium-doped octacalcium phosphate and hydroxyapatite thin films using pulsed laser depostion. *J Biomed Mater Res B Appl Biomater*. 2015; 103: 151-158.

22. Gulati K, Prideaux M, Kogawa M, Lima-Marques L, Atkins GJ, Findlay DM *et al.* Anodized 3D-printed titanium implants with dual micro- and nano-scale topography promote interaction with human osteoblasts and osteocyte-like cells. *J Tissue Eng Regen Med*. 2017; 11: 3313-3325.

23. Nune KC, Misra R, Gai X, Li SJ, Hao YL. Surface nanotopography-induced favorable modulation of bioactivity and osteoconductive potential of anodized 3D printed Ti-6Al-4V alloy mesh structure. *J Biomater Appl*. 2018; 32: 1032-1048.

24. Li LH, Kong YM, Kim HW, Kim YW, Kim HE, Heo SJ *et al.* Improved biological performance of Ti implants due to surface modification by micro-arc oxidation. *Biomaterials*. 2004; 25: 2867-2875.

25. Marques I, Alfaro MF, Cruz NCD, Mesquita MF, Takoudis C, Sukotjo C *et al.* Tribocorrosion behavior of biofunctional titanium oxide films produced by micro-arc

oxidation: Synergism and mechanisms. *Journal of the mechanical behavior of biomedical materials*. 2016; 60: 8-21.

26. Ribeiro AR, Oliveira F, Boldrini LC, Leite PE, Falagan-Lotsch P, Linhares AB *et al.* Micro-arc oxidation as a tool to develop multifunctional calcium-rich surfaces for dental implant applications. *Materials science & engineering C, Materials for biological applications*. 2015; 54: 196-206.

27. Xu L, Zhang K, Wu C, Lei X, Ding J, Shi X *et al.* Micro-Arc Oxidation Enhances the Blood Compatibility of Ultrafine-Grained Pure Titanium. *Materials (Basel, Switzerland)*. 2017; 10.

28. Jin B, Choung PH. Recombinant Human Plasminogen Activator Inhibitor-1 Accelerates Odontoblastic Differentiation of Human Stem Cells from Apical Papilla. *Tissue Eng Part A*. 2016; 22: 721-732.

29. Martins R, Cestari TM, Arantes RVN, Santos PS, Taga R, Carbonari MJ *et al.* Osseointegration of zirconia and titanium implants in a rabbit tibiae model evaluated by microtomography, histomorphometry and fluorochrome labeling analyses. *Journal of periodontal research*. 2018; 53: 210-221.

30. Park JY, Choi JC, Shim JH, Lee JS, Park H, Kim SW *et al.* A comparative study on collagen type I and hyaluronic acid dependent cell behavior for osteochondral tissue bioprinting. *Biofabrication*. 2014; 6: 035004.

31. Shim JH, Kim JY, Park M, Park J, Cho DW. Development of a hybrid scaffold with synthetic biomaterials and hydrogel using solid freeform fabrication technology. *Biofabrication*. 2011; 3: 034102.

32. Shim JH, Jang KM, Hahn SK, Park JY, Jung H, Oh K *et al.* Three-dimensional bioprinting of multilayered constructs containing human mesenchymal stromal cells for osteochondral tissue regeneration in the rabbit knee joint. *Biofabrication*. 2016; 8: 014102.

33. Parolini O, Alviano F, Bagnara GP, Bilic G, Buhring HJ, Evangelista M *et al.* Concise review: isolation and characterization of cells from human term placenta: outcome of the first international Workshop on Placenta Derived Stem Cells. *Stem Cells*. 2008; 26: 300-311.

34. Dominici M, Le Blanc K, Mueller I, Slaper-Cortenbach I, Marini F, Krause D *et al.* Minimal criteria for defining multipotent mesenchymal stromal cells. The International Society for Cellular Therapy position statement. *Cytotherapy*. 2006; 8: 315-317.

35. Pobloth AM, Checa S, Razi H, Petersen A, Weaver JC, Schmidt-Bleek K *et al.* Mechanobiologically optimized 3D titanium-mesh scaffolds enhance bone regeneration in critical segmental defects in sheep. *Science translational medicine*. 2018; 10.

36. Foley BD, Thayer WP, Honeybrook A, McKenna S, Press S. Mandibular reconstruction using computer-aided design and computer-aided manufacturing: an analysis of surgical results. *J Oral Maxillofac Surg*. 2013; 71: e111-119.

37. Hanasono MM, Skoracki RJ. Computer-assisted design and rapid prototype modeling in microvascular mandible reconstruction. *Laryngoscope*. 2013; 123: 597-604.

38. Wang N, Li H, Lu W, Li J, Wang J, Zhang Z *et al.* Effects of TiO2 nanotubes with different diameters on gene expression and osseointegration of implants in minipigs. *Biomaterials*. 2011; 32: 6900-6911.

39. Mendonca G, Mendonca DB, Simoes LG, Araujo AL, Leite ER, Duarte WR *et al.* The effects of implant surface nanoscale features on osteoblast-specific gene expression. *Biomaterials*. 2009; 30: 4053-4062.

40. Fuller K, Wong B, Fox S, Choi Y, Chambers TJ. TRANCE is necessary and sufficient for osteoblast-mediated

activation of bone resorption in osteoclasts. *The Journal of experimental medicine*. 1998; 188: 997-1001.

41. Simonet WS, Lacey DL, Dunstan CR, Kelley M, Chang MS, Luthy R *et al.* Osteoprotegerin: a novel secreted protein involved in the regulation of bone density. *Cell*. 1997; 89: 309-319.

42. Tsuda E, Goto M, Mochizuki S, Yano K, Kobayashi F, Morinaga T *et al.* Isolation of a novel cytokine from human fibroblasts that specifically inhibits osteoclastogenesis. *Biochemical and biophysical research communications*. 1997; 234: 137-142.

43. Anderson DM, Maraskovsky E, Billingsley WL, Dougall WC, Tometsko ME, Roux ER *et al.* A homologue of the TNF receptor and its ligand enhance T-cell growth and dendritic-cell function. *Nature*. 1997; 390: 175-179.

44. Arnoldi J, Alves A, Procter P. Early tissue responses to zoledronate, locally delivered by bone screw, into a compromised cancellous bone site: a pilot study. *BMC musculoskeletal disorders*. 2014; 15: 97.

45. Washio K, Tsutsumi Y, Tsumanuma Y, Yano K, Srithanyarat SS, Takagi R *et al.* In Vivo Periodontium Formation Around Titanium Implants Using Periodontal Ligament Cell Sheet. *Tissue Eng Part A*. 2018; 24:

1273-1282.

46. Seo BM, Miura M, Gronthos S, Bartold PM, Batouli S, Brahim J *et al.* Investigation of multipotent postnatal stem cells from human periodontal ligament. *Lancet (London, England)*. 2004; 364: 149-155.

47. Nakajima K, Oshima M, Yamamoto N, Tanaka C, Koitabashi R, Inoue T *et al.* Development of a Functional Biohybrid Implant Formed from Periodontal Tissue Utilizing Bioengineering Technology. *Tissue Eng Part A*. 2016; 22: 1108-1115.

48. Buser D, Warrer K, Karring T. Formation of a periodontal ligament around titanium implants. *J Periodontol*. 1990; 61: 597-601.

49. Giannobile WV. Getting to the root of dental implant tissue engineering. *Journal of clinical periodontology*. 2010; 37: 747-749.

50. Kim BS, Kwon YW, Kong JS, Park GT, Gao G, Han W *et al.* 3D cell printing of in vitro stabilized skin model and in vivo pre-vascularized skin patch using tissue-specific extracellular matrix bioink: A step towards advanced skin tissue engineering. *Biomaterials*. 2018; 168: 38-53.

51. Singh D, Thomas D. Advances in medical polymer technology towards the panacea of complex 3D tissue

and organ manufacture. *American journal of surgery*. 2018.

52. Hoz L, Romo E, Zeichner-David M, Sanz M, Nunez J, Gaitan L *et al.* Cementum protein 1 (CEMP1) induces differentiation by human periodontal ligament cells under three-dimensional culture conditions. *Cell biology international*. 2012; 36: 129-136.

53. Alvarez-Perez MA, Narayanan S, Zeichner-David M, Rodriguez Carmona B, Arzate H. Molecular cloning, expression and immunolocalization of a novel human cementum-derived protein (CP-23). *Bone*. 2006; 38: 409-419.

Figure Legends and Figures

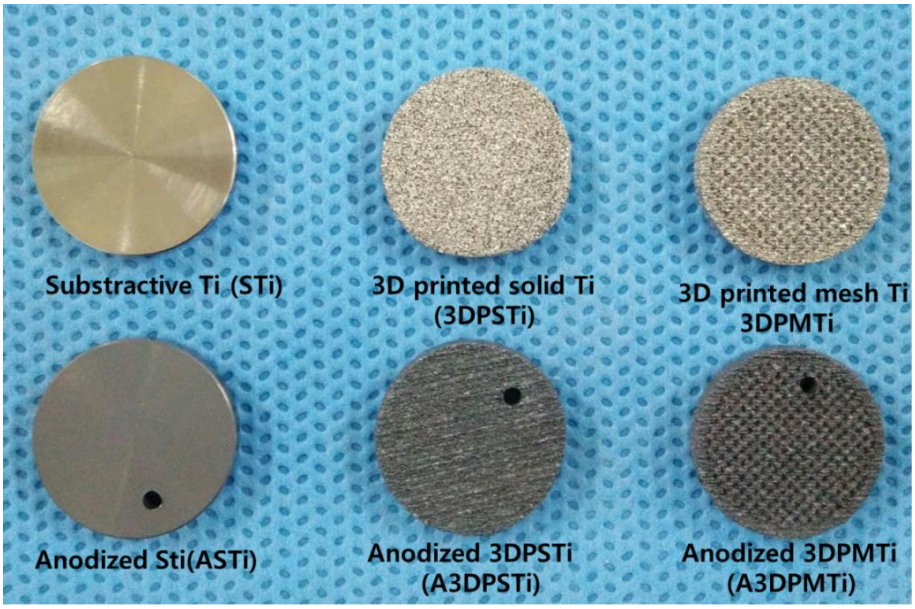

Figure 1. In vitro test samples

The porous structures were based on dode-thin unit cells in the MAGICS program with the following design (nominal) dimensions: strut size = 120 μm, pore size = 500 μm, porosity = 88%.

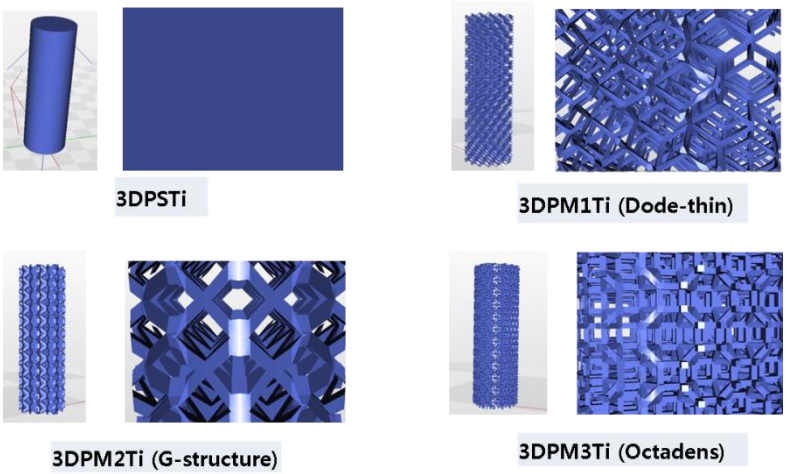

Figure 2. Mesh configuration of *in vivo* specimens for implantation in rabbit

5 types of specimens (Ø2.5 mm x6.0 mm) were manufactured, 4 types (soild, dode-thin, octadense, and G-structure) by additive manufacturing and one sample manufactured by subtractive manufacturing.

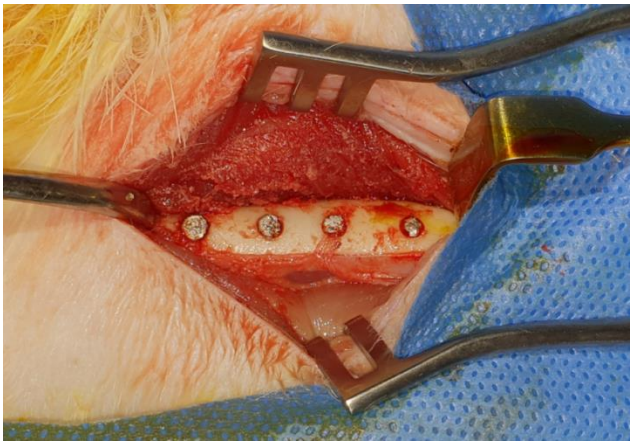

Figure 3. Drilling to the rabbit femur and inserted 3D printed implant.

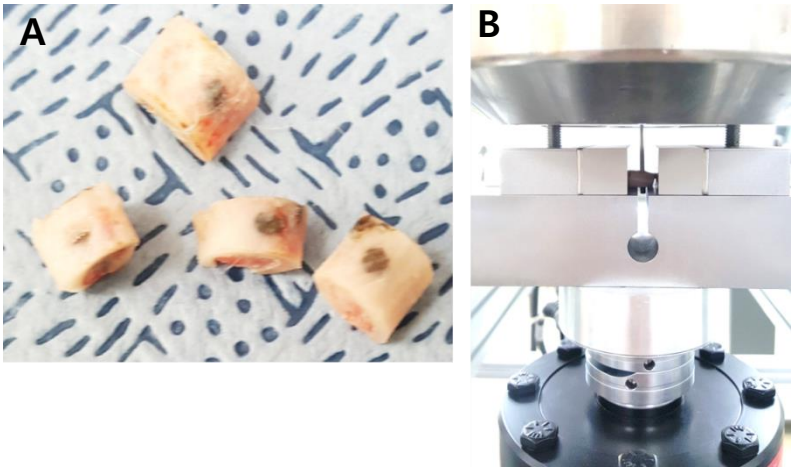

Figure 4. A. specimens inserted in rabbit femur. B. Setup for Push-out test.

This process was performed by ISO10993-6:2007 (tests for local effects after implantation, Annex D-Test method for implantation in bone). The enucleated portion was fixed to a jig, and the push-out test was performed (Instron 5966, Illinois Tool Works Inc., USA) in the same rod as specimen size (Ø 2.5 mm).

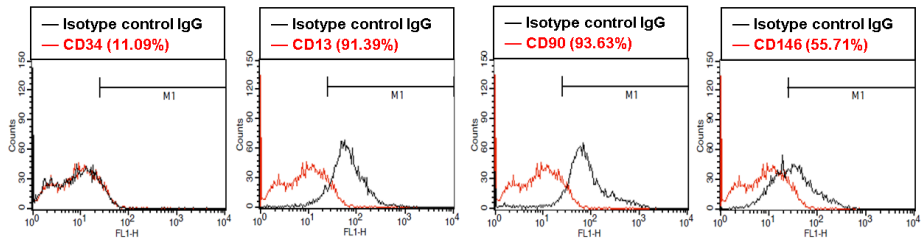

Figure 5. Fluorescence-activated cell sorting analysis of hBMSC

Flow cytometric analysis showed that approximately 91.39% of the hBMSC expressed CD13, 93.63% expressed CD90, 55.71% expressed CD146, and 11.09% expressed CD34.

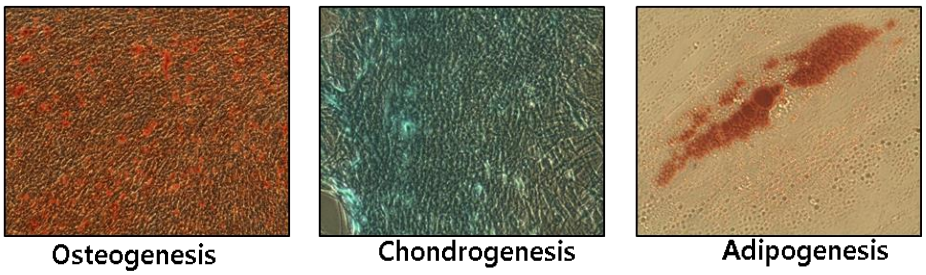

Figure 6. Multilineage differentiation capacity of hBMSC *in vitro* with osteogenic, chondrogenic, and adipogenic medium

After 3 weeks of osteogenic and adipogenic induction, hBMSCs formed extensive Alizarin red S-positive mineral deposits and Oil Red O-positive lipid droplets throughout the adherent layers. Furthermore, hBMSCs also formed Alcian Blue-positive nodules after incubation in chondrogenic induction medium.

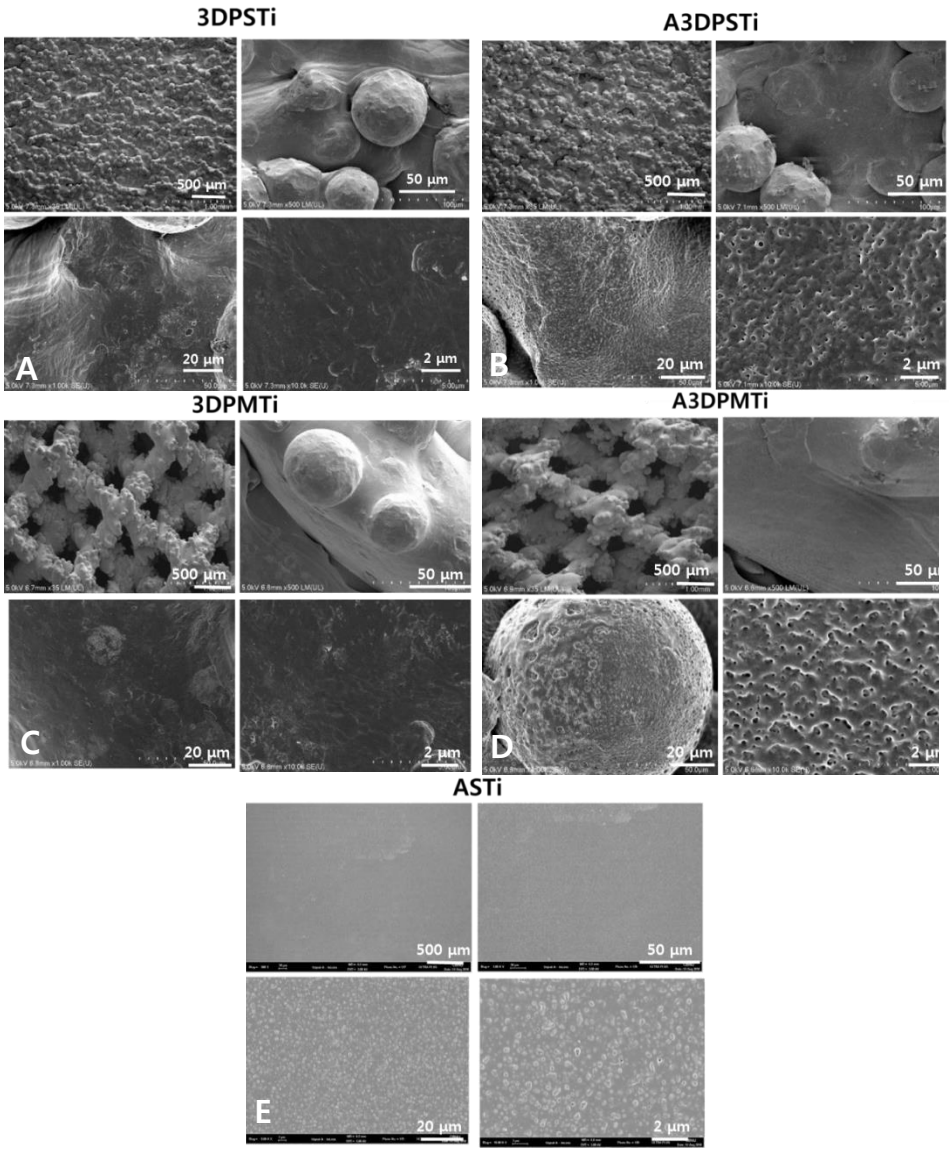

Figure 7A–E. Surface characterization of 3D–printed solid titanium (3DPSTi), anodized 3D–printed solid titanium (A3DPSTi), 3D–printed mesh titanium (3DPMTi), anodized 3D–printed mesh titanium (A3DPSTi), anodized substractive titanium (ASTi). Scanning electron micrograph (SEM) images.

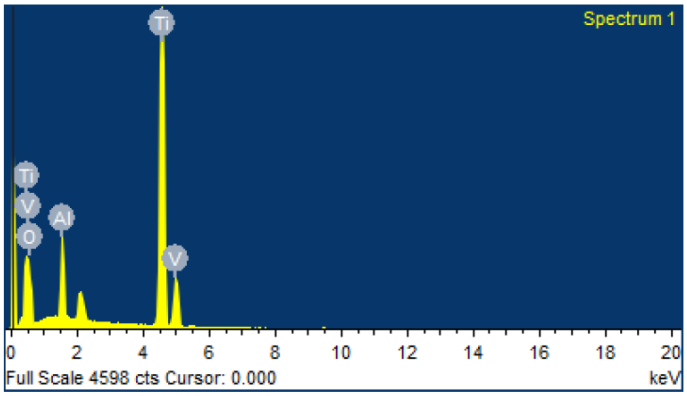

Element	Weight%	Atomic%
O K	20.95	42.93
Al K	5.79	7.04
Ti K	70.78	48.44
V K	2.47	1.59
Totals	100.00	

Figure 8. Energy disperse spectroscopy (EDS) of anodized sample

The chemical constitution and state of the components in the 3D printed sample surface after microarc oxidation was characterized by energy disperse spectroscopy (EDS). According to the EDS, the main surface components are O, Ti, Al, and V.

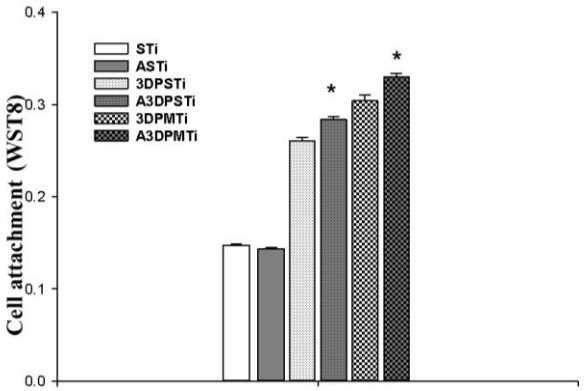

Figure 9. Cell adhesion assay

Cell adhesion efficacy was found to be: anodized 3D printed mesh titanium (A3DPMTi) > 3D printed mesh titanium (3DPMTi) > anodized 3D printed solid titanium (A3DPSTi) > 3D printed solid titanium (3DPSTi) > subtractive titanium (STi) = anodized subtractive titanium (ASTi). * $p<0.05$

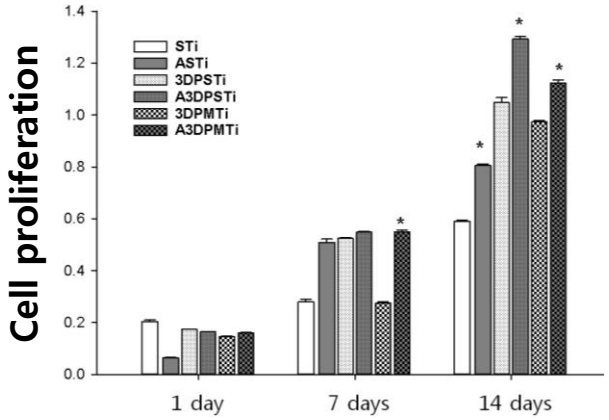

Figure 10. The WST-8 assay

The WST-8 assay of 1 day and 7 day cultures identified no significant difference in the number of cells between the groups. Anodized group showed significantly higher cell proliferation as compared to non-anodized groups at 14 days. * $p<0.05$

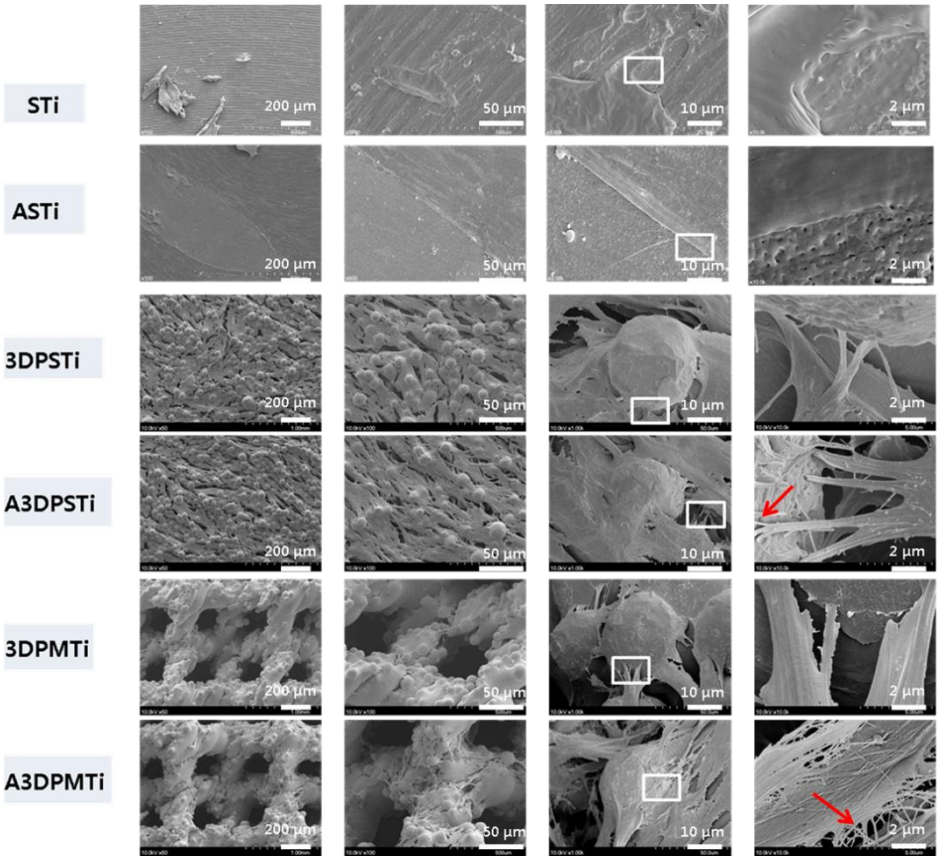

Figure 11. Scanning Electron Microscopy

At 7 days, cellular extensions were observed between micro-particles, and also entering into the nanopores that was shown on the surface of anodized samples. Surface morphology of the anodized additive manufactured samples, with micro-scale micro–particles, in associated with nanoporous coating, produces a surface that enhances strong anchoring (arrow) of the hBMSCs.

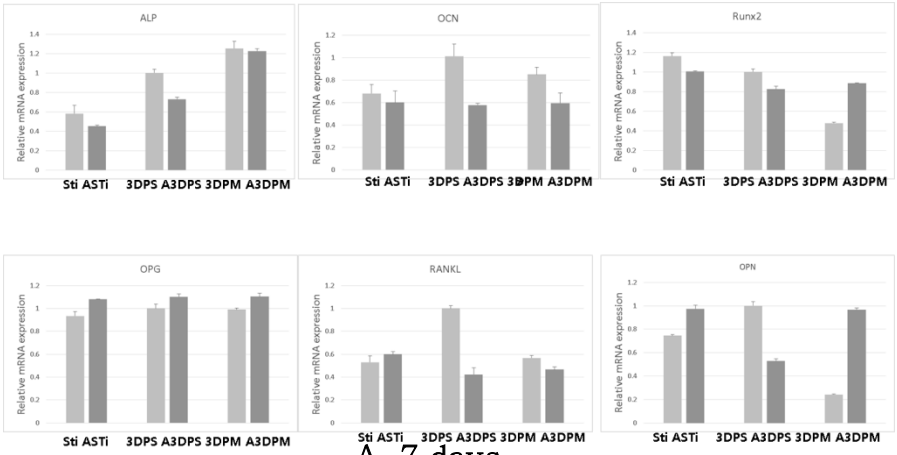

A. 7 days

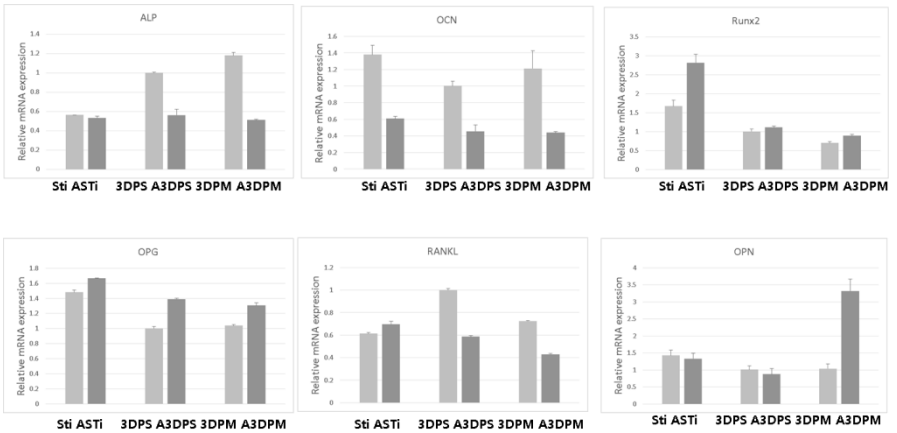

B. 14 days

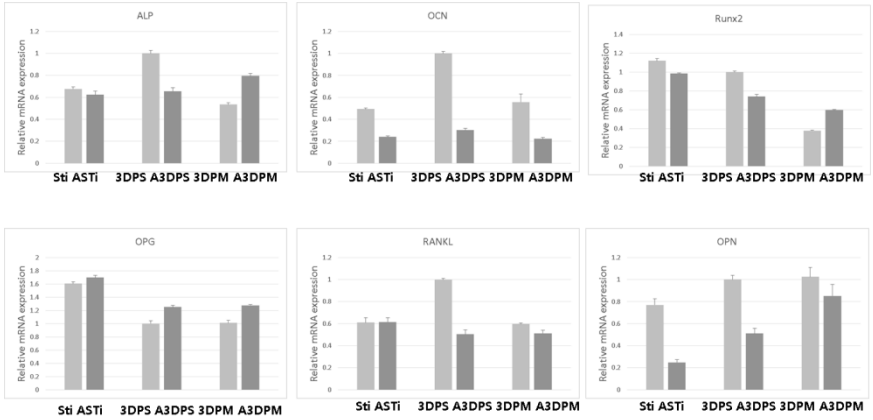

C. 21 days

Figure 12. Real-time PCR

Expression of ALP, OCN, Runx2, OPG, RANKL, and OPN measured based on relative mRNA expression after 7, 14, and 21 days of call culture with real-time PCR. ALP, Runx2, RANKL, and OPG did not show any particular differences between both groups. After 14 days, the expression of ALP, OCN, and RANKL in the 3D printed non-anodized group was higher than in the anodized group. However anodized 3D printed mesh titanium (A3DPMT) exhibited greater expression of OPN as compared to non-anodized surfaces. The relative expression of OPG was elevated in cells cultured on anodized samples (Fig. 12B). At Day 21, the expression of the osteoclastogenic inhibitory factor OPG was elevated on anodized surfaces (Fig. 12C). Anodized surfaces also showed lowered expression of RANKL, OCN, and OPN (Fig. 12C).

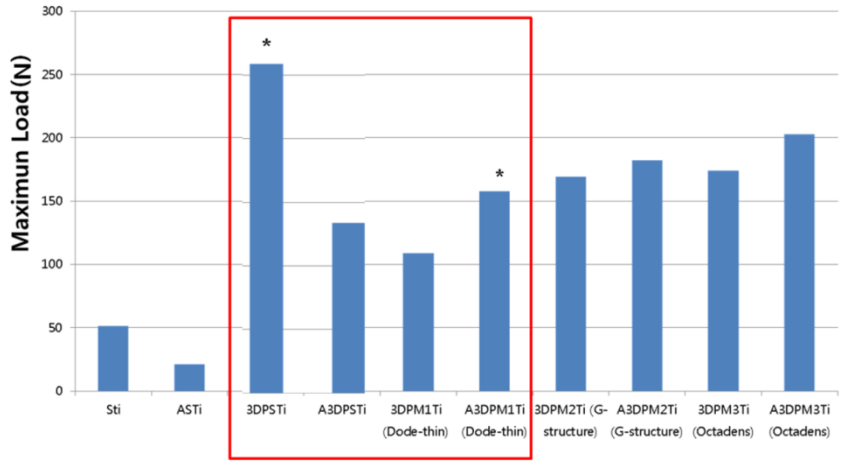

Figure 13. Push-out test

The 3D printed group was found to withstand a higher load than the subtractive manufacturing group. 3D printed solid group was found to withstand a highest load about 260 N.

* $p<0.05$

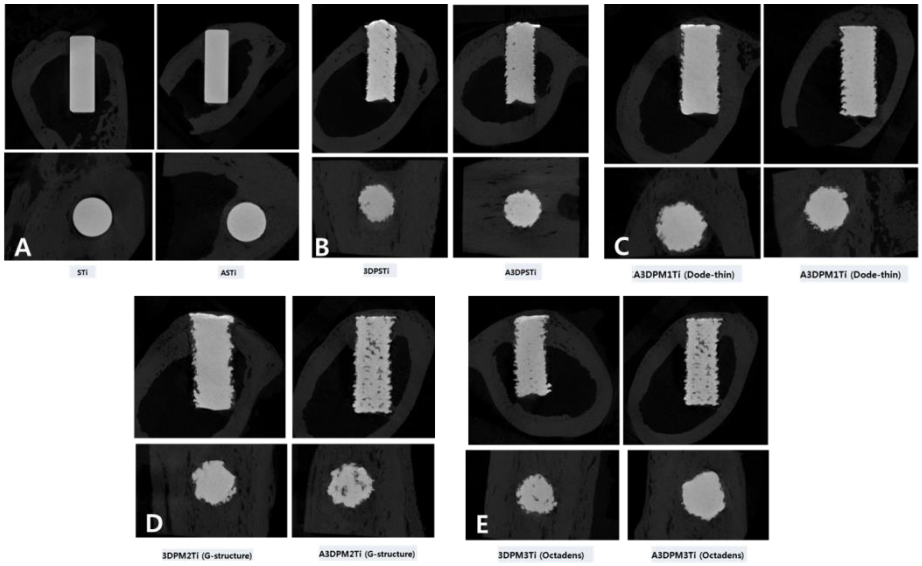

Figure 14. Micro CT images

After 6 weeks of healing, all implants were in close contact with the surrounding bone except subtractive titanium (STi) by Micro-CT.

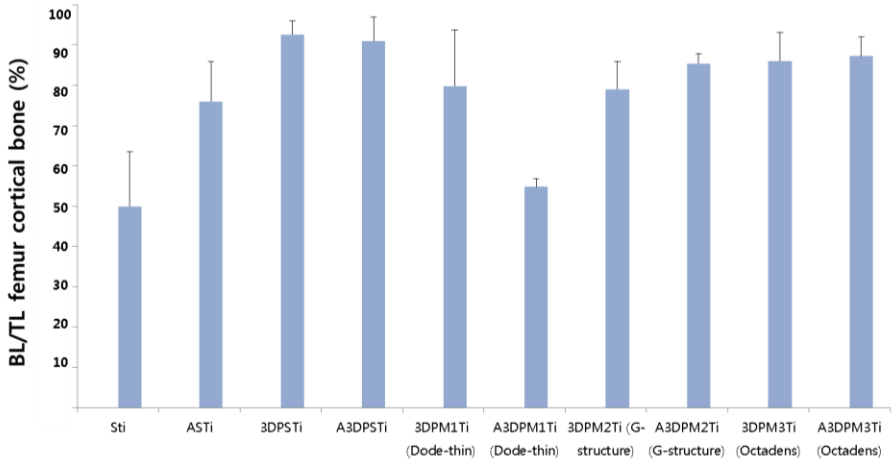

Figure 15. Ratio of the total length of each sample (TL) and length of the portion in contact with the bone (BL) by micro-CT

The BL/TL of the cortical femur bone in the Sti (49.9 %) was lowest value and in the 3DPSTi (92.5 %) was the highest value. Micro-CT analysis did not show any particular differences between non-anodized and anodized groups.

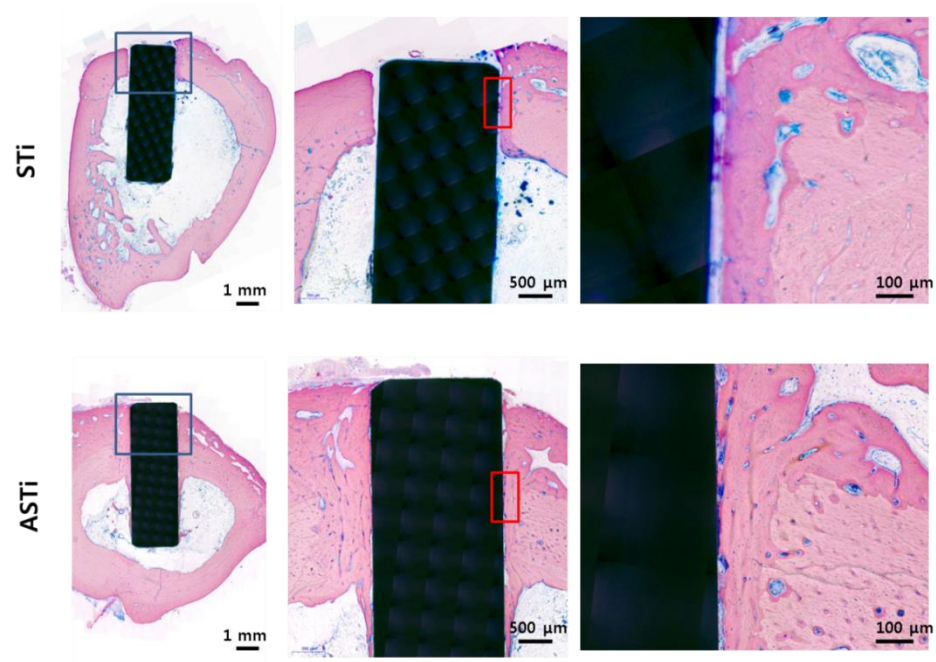

Figure 16. Histologic sections of Sti and ASTi with basic fuchsin stain.

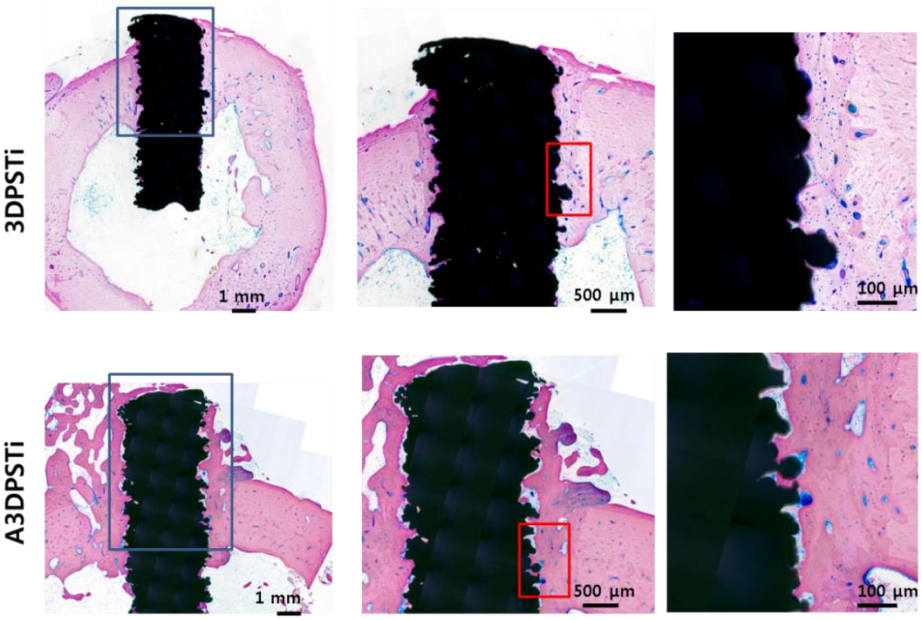

Figure 17. Histologic sections of 3DPSTi and A3DPSTi with basic fuchsin stain.

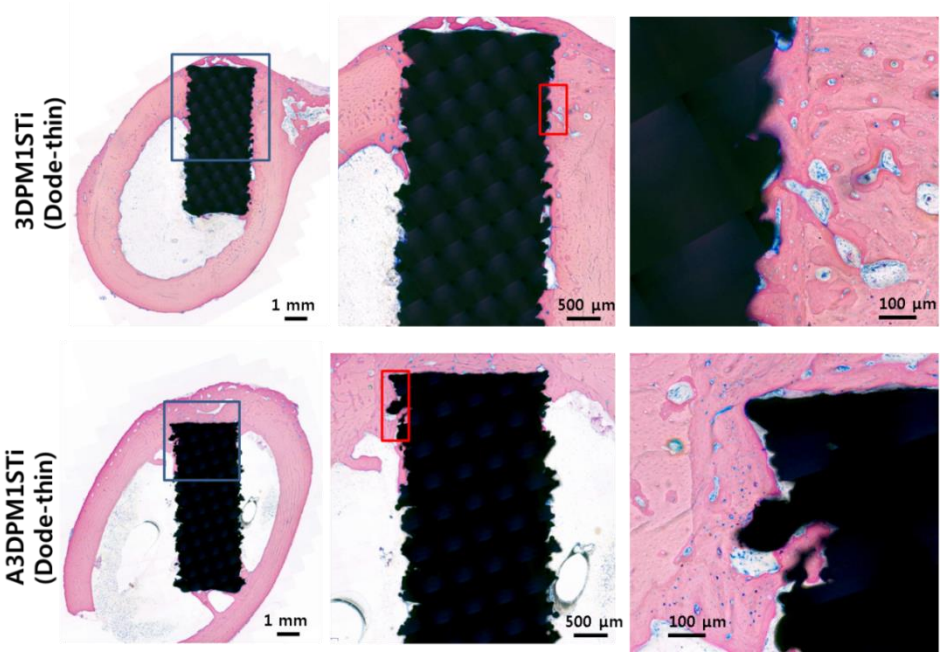

Figure 18. Histologic sections of 3DPM1Ti and A3DPM1Ti with basic fuchsin stain.

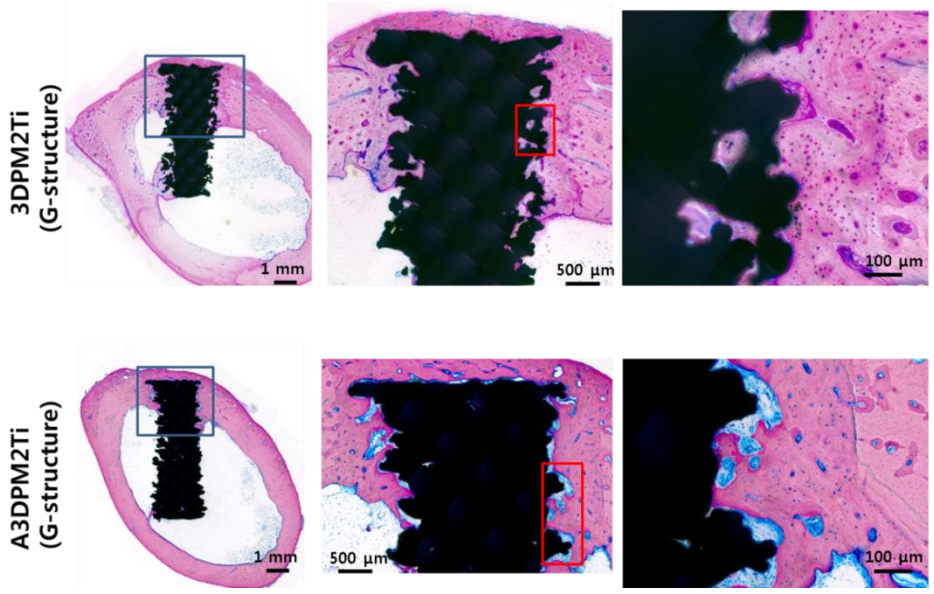

Figure 19. Histologic sections of 3DPM2Ti and A3DPM2STi with basic fuchsin stain.

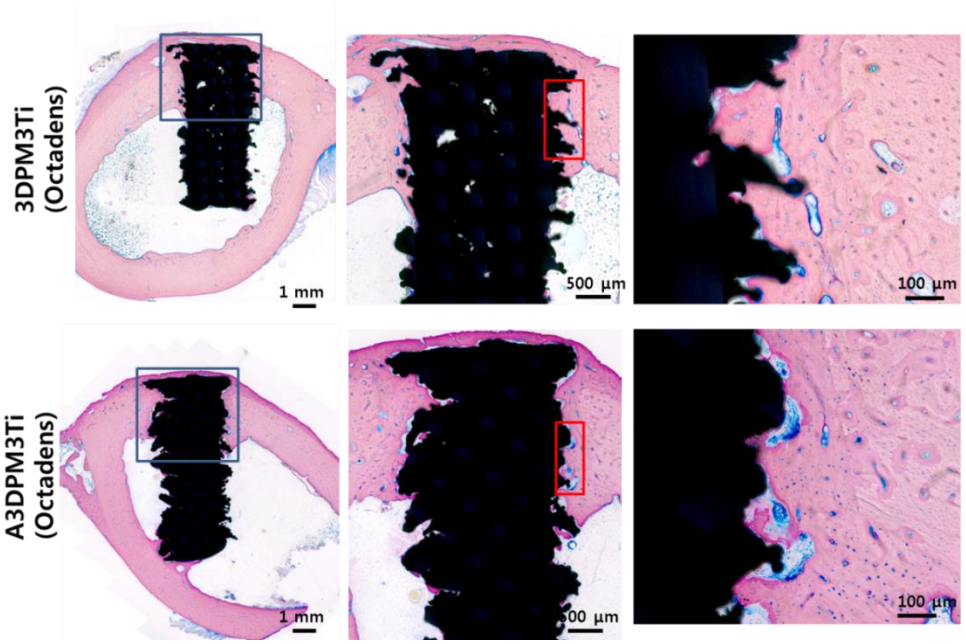

Figure 20. Histologic sections of 3DPM3Ti and A3DPM3Ti with basic fuchsin stain.

Tables

Target cDNA	Forward Primer sequence (5’ –3’)	Reverse Primer sequence (5’ –3’)
ALP	TAAGGACATCGCCTACCAGCTC	TCTTCCAGGTGTCAACGAGGT
Runx2	CTTTACTTACACCCCGCCAGTC	AGAGATATGGAGTGCTGCTGGTC
OPN	CAGCCATGAATTTCACAGCC	GGGAGTTTCCATGAAGCCAC
OCN	TGAGAGCCCTCACACTCCTC	ACCTTTGCTGGACTCTGCAC
RANKL	GGGTGGAGGTGTACTATGATGG	CTTGCCGTAGGAGGAGCTG
OPG	CCACTACGACCTACTGGATGC	GTTGCCGAAGTCACAGGTG
GAPDH	CTTTGGTATCGTGGAAGGACTC	GTAGAGGCAGGGATGATGTTCT

Table 1. Primer sequences for real–time PCR

Part II. Impact of bioprinting on titanium 3D printed porous scaffold in periodontal ligament regeneration

I. Introduction

Tumor resection, trauma, osteoradionecrosis, and various other causes may result in maxillofacial bone defects. The ultimate goal of reconstruction of maxillofacial bone defects is to restore bone defects, restore facial shape to its original form, minimize malocclusion, and restore masticatory function. In addition, the goal is to minimize the morbidity of donor and recipient and to perform reconstruction with minimum number of operations.[1, 2] Development of CAD-CAM technology and electron beam melting (EBM) with adequate strength and biocompatibility makes the foundations for application of titanium patient-specific 3-dimensional printed implants in the field of maxillofacial bone reconstruction.[3-5] In fact, multicenter study about using patient-specific CAD/CAM reconstruction plates for mandibular reconstruction has been performed with good results,[6] while a case was reported on successful

reconstruction of maxillomandibular defect using 3D printed titanium mesh.[7]

The problem that is expected when reconstructing jaws with 3D printed titanium is oral side exposure. Since the oral mucosa is thin and fat layer is absent, infection may occur with saliva during exposure. When the titanium implant part is exposed, it can be solved by washing the infected 3D printed structure well and water tight wound closure with suture same as treatment of peri-implantitis. But if the infection is spread on the implant-bone interface by exposing the site connected with the existing bone, the implant can be removed.

To solve the problem, 3D printed hybrid artificial organ was fabricated by combining EBM technology and bioprinting of periodontal ligament in this study. Osseointegrated dental implants have been recognized as being very reliable and having long-term predictability. However, host defense mechanisms against infection have been known to be impaired around a dental implant because of the lack of a periodontal ligament (PDL).[2, 8] The PDL protects against infection and protect against bone resorption associated with mechanical stress, such as traumatic occlusal force and orthodontic tooth movement.[9, 10]

Organ functions are performed through biological cooperation

with adjacent tissues and other organs.[11] Fibrous connective tissues, such as muscles, tendons and periodontal ligaments, is essential in achieving biological organ functions, including tight connectivity, mobility and resistance against mechanical stimulations and infections.[12] When reconstructing a mandibular segmental defect with a titanium 3D printed implant, there is a surface that contacts the implant and the existing bone. Reconstruction with 3D printed hybrid artificial organ can be done to prevent infection if the fibrous connective tissue, such as periodontal ligament is interposed between the titanium implant and the bone in the area close to oral mucosa and the osseointegration is obtained at the area contacting the basal bone at the lower part. 3D printed hybrid artificial organ can also be applied to dental implants. 3D printed hybrid dental implant could establish physiological tooth functions, including the ability to react to mechanical stimulus and the ability to resist to infection. Many studies have demonstrated that periodontal ligament stem cells (PDLSCs) have ability of self-renewal and differentiation, clonogenicity, and capacity to produce connective tissue between cementum and bone.[13-16] Currently 3D cell-printing technique has been utilized as new biofabrication platform because of its ability to locate living cells in pre-defined spatial locations with scaffold and various

growth factors.[17] In this study, we tried PDL regeneration on 3D printed titanium structure's surface using hPDLSCs bioprinting technique for fabricating 3D printed hybrid artificial organ.

II. Materials and Methods

1. Primary cell culture from extracted human third molar

Non-decayed human third molars that had been impacted in the mandible were extracted from 5 adults (18-28 years of age) under informed consent at the Seoul National University Dental Hospital, Seoul, South Korea. The experimental protocol was approved by the Institutional Review Board of the hospital (IRB No. 05004). Periodontal ligament was gently separated from the root of extracted third molars and the separated tissues were digested in a solution of 3 mg/mL collagenase type I (Worthington Biochem, Freehold, NJ) and 4 mg/mL dispase (Boehringer, Mannheim, Germany) for 1 h at 37C. Single-cell suspensions were collected by passing the cells through a 40-mm strainer (Falcon BD Labware, Franklin Lakes, NJ) and were cultured in the alpha-modification of Eagle's medium (alpha-MEM; Gibco BRL, Grand Island, NY) supplemented with 10% fetal bovine serum (Gibco BRL), 100 mM ascorbic acid 2-phosphate (Sigma-Aldrich, St. Louis, MO), 2mM glutamine, 100 U/mL penicillin, and 100 mg/mL streptomycin (Biofluids, Rockville, MD) and. The medium was changed after the first 24 h and then every 3 days. Three colonies of human periodontal

ligament stem cells (hPDLSCs) were randomly picked and the cellular pool of those colonies was used for in vitro proliferation, differentiation studies, and animal experiment. All primary cells used in this study were in passage 2 or 3.

2. Flow cytometric analysis of the hPDLSCs

To characterize the immunophenotype of the hPDLSCs, the expression of mesenchymal stem cell-associated surface markers at passage 3 was analyzed by flow cytometry as previously reported.[18] hPDLSCs in their third passage (1.0×10^6 cells) were fixed with 3.7% paraformaldehyde from 95% paraformaldehyde powder (Sigma-Aldrich) diluted in phosphate-buffered saline (PBS) (3.7 g/100 mL) for 10 min and re-suspended in PBS containing 1% bovine serum albumin (BSA) (ICN Biomedicals) for 30 min for blocking nonspecific antibody-binding sites. hPDLSCs were then incubated with specific antibodies against CD34, CD13, CD90, or CD146 at 4° C for 1 h, and then incubated with fluorescent secondary antibodies at room temperature for 1 h. All used antibodies were purchased from BD Biosciences. We measured the percentages of CD13-positive, CD90-positive, CD146-positive, and CD34-negative cells using a FACS Calibur flow cytometer (Becton Dickinson Immunocytometry Systems). We

analyzed the results using CellQuest Pro software (Becton Dickinson).

3. Osteogenic, chondrogenic, and adipogenic differentiation of the hPDLSCs

To promote osteogenic, chondrogenic, and adipogenic differentiation, hPDLSCs were cultured in StemPro Osteogenic, StemPro Chondrogenic, and StemPro Adipogenic differentiation medium (Gibco BRL), respectively, with the appropriate supplements as previously reported.[18]. At 21 days, the cells with postosteogenic, postchondrogenic, and postadipogenic induction were stained with 2% Alizarin Red S stain at pH 4.2 (Sigma-Aldrich), 1% Alcian Blue (Sigma-Aldrich), and 0.3% Oil Red O dye (Sigma-Aldrich) to detect proteoglycans, Nissl bodies, and fat vacuoles as indicators of osteogenic, chondrogenic, and adipogenic differentiation, respectively. Stained cells were visualized under an inverted light microscope (Olympus U-SPT; Olympus).

4. Titanium 3D printing scaffold manufacturing for hPDLSCs printing

Two CAD/CAM programs (3-Matic/MAGICS, Materialise, Belgium) to design a 3D printed implant for hPDLSCs printing

were utilized. The porous structures were based on dode-thin unit cells in the MAGICS program with the following design (nominal) dimensions: strut size = 120 μm, pore size = 500 μm, porosity = 88%. Disk-shaped samples with size (Ø8mm x H2 mm, Ø18 mm x H2 mm) were designed. The designed STL file was programmed to a 3D printer with an EBM method of metal additive manufacturing (Arcam A1, Arcam, Sweden), and samples were printed using Ti-6Al-4 V-ELI medical grade powder (Arcam A1, Arcam, Sweden) as previously described.

5. Preparation of hPDLSCs bioinks.

A commercial atelo-collagen (MS collagen, MSBIO Inc. Republic of Korea) and recombinant human fibroblast growth factor basic-2 (FGF-2, ProSpec, Israel) were prepared. The experimental groups used in this study were 5% (wt/v) collagen only and 5% collagen mixed with 10 ng/ml FGF-2. For bioprinting of a periodontal ligament (PDL) layer, bioinks were made by mixing the above two biomaterials and hPDLSCs. The final cell concentration in the bioink was $1x10^7$ cells/ml.

6. Bioprinting process for periodontal ligament regeneration

Scaffolds fabricated by titanium 3D printing were prepared for

bioprinting of PDL layer. In this study, experimental groups were classified according to cell seeding and cell printing methods. In the cell seeding group, collagen or collagen with FGF-2 were printed one layer on a titanium scaffold surface and stored for 30 min at 37℃ for gelation. After that, hPDLSCs were seeded on the printed bioink without cells (group 1: titanium scaffold/collagen/cell seeding, group 2: titanium scaffold/collagen+FGF-2/cell seeding). In the cell printing group, the bioinks with cells (group 3: titanium scaffold/collagen/cell printing, group 4: titanium scaffold/collagen+FGF-2/cell printing) were printed one layer on a titanium scaffold surface and stored for 30 min at 37℃ for gelation (Fig. 1). For precise cell printing experiment, we used a bioprinter (3DX Printer, T&R Biofab Co., Ltd., Republic of Korea) (Fig. 2). Bioprinting using a nozzle was performed with an inner diameter of 400 μm. All samples were cultured in the alpha-modification of Eagle's medium (alpha- MEM; Gibco BRL, Grand Island, NY) supplemented with 10% fetal bovine serum (Gibco BRL), 100 mM ascorbic acid 2-phosphate (Sigma-Aldrich, St. Louis, MO), 2mM glutamine, 100 U/mL penicillin, and 100 mg/mL streptomycin (Biofluids, Rockville, MD) and. The medium was changed after the first 24 h and then every 3 days and incubated at 37C in 5% CO_2.

7. Scanning Electron Microscopy (SEM) and sample observation

4 groups of samples were fixed with modified Karnovsky's fixative for 2 hours. The samples were washed 3 times with PBS buffer for 15 min and fixed with 1% osmium tetroxide (EMS). The samples were then washed with distilled water and dehydrated with graded concentrations (70, 80, 90, 95 and 100% v/v) of ethanol. The samples were then treated with hexamethyl disilazane (HMDS) for 20 min. Finally, the samples were coated with Pt prior to cell shape observation with field emission scanning electron microscope (FE-SEM; Hitachi S-4700) using an acceleration voltage of 15kV at three different magnifications: x10000, x1000, x 50.We cultured the four groups of samples for up to 21 days incubated at 37C in 5% CO_2 in order to determine how long the gelled collagen printed on the scaffold retained its shape and took pictures every day.

8. Live/dead cell assay and proliferation assay

The viability of seeded and printed hPDLSCs was evaluated by live/dead cell assay kit (Lonza, Walersville, MD, USA).[19] We also confirmed by live / dead assay that the cells were uniformly located on the scaffold surface. We observed live and

dead cells, which were revealed by calcein AM (green) and EthD-1 (Red), respectively[19] by confocal microscope (IX81; Olympus, Tokyo, Japan). Proliferation of seeded and printed hPDLSCs was analyzed using a CCK-8 (Dojindo, Japan), as reported previously.[20] 4 group of samples were cultured for 1, 4, 7 days. We quantified viable cells by measuring the optical density of the CCK-8 solution at 450 nm with a microplate reader (UVM 340; Olympus,Tokyo,Japan).[21]

9. Evaluation of the differentiation of seeded and printed hPDLSCs by real-time PCR

To evaluate periodontal ligament gene expression levels, 4 group of samples cultured for 7 days as under without any induction. Total RNA was prepared using an RNeasy Mini Kit (Qiagen) according to the manufacturer's instructions, and cDNA was synthesized from 1 μg of total RNA using reverse transcriptase (Superscript II Preamplification System; Invitrogen). Oligonucleotide primers for the amplification of human ALP, Cemp1, and Col1 mRNA were designed. Real-time polymerase chain reaction (PCR) was performed with SYBR Green PCR Master Mix (ABI Prism 7500 sequence detection system; Applied Biosystems). The reaction conditions were 40 cycles of 15 s of denaturation at 95° C and one min of

amplification at 60° C. All reactions were run in triplicate and were normalized to the reference gene (GAPDH). The specific primer sets used for this analysis are listed in Table 1.

10. Animal experiments in athymic rat for evaluating PDL regeneration *in vivo*

Surgical Procedures

Athymic rats (Hsd:RH-Foxn1Rnu , 10 males, 9 weeks old, Envigo, New Jersey, USA) were used for the animal experiment of transplantation of 3D printed titanium scaffold with seeded or cell printed hPDLSCs into a calvarial bone defect. The study protocol was approved by the Ethics Committee on Animal Experimentation of Chung-Ang University. After the rats were anesthetized with alfaxanolone (Alfaxan® ,Jurox, Australia) (3 mg/kg) and xylazine hydrochloride (Rompun® ,Bayer Korea, Korea) (10 ml/kg) IP. To access the cranial vault of the rat, a 4 cm incision was made in the skin with number 15 blade in the middle region of the skull. The skin, facial and the periosteum were dissected and we got enough access to calvaria. Using 8 mm trephine bur, we made 2 circular shaped bone ditches not penetrated into dura with a diameter of 8 mm. And using round bur, a bony pit with a depth of 1.5 mm inside the circle was made on calvaria. We

transplanted 4 groups of samples after 2 days of incubation with cells layer in contact with the calvarial bone (Fig. 3). After transplantation, the surgical wound was sutured with 4-0 nylon. Six weeks after transplantation, the rats were euthanized, and the calvaria with implanted specimens were harvested (Fig. 4).

Histologic preparation for undecalcified sections

Specimens were dehydrated in a graded concentration of ethanol and embedded in methyl methacrylate resin (Technovit® 7200; Heraeus Kulzer, Wehrheim, Germany). Blocks of methyl methacrylate including the samples were sectioned at 100-㎛ thickness in the sample's long axis using a diamond-coated saw cutter and the Exakt grinding system (EXAKT Advanced Technologies GmbH, Norderstedt, Germany). And followed by the sections were further ground and polished to 20-㎛ thickness. The sections were then stained with H&E and basic fuchsin, by which the bone was stained red.

Histologic preparation for decalcified sections and Immunohistochemistry

H&E staining and immunofluorescence staining of periostin, HLA class I, vWF, and Cemp1.were performed. For the analyses, enucleated calvaria were fixed with 4%

paraformaldehyde solution and decalcified using 10% sodium citrate and 22.5% formic acid for 2 weeks at 4 °C. Staining was performed on 6 μm paraffin-embedded sections. After deparaffinization, the slides were incubated with Proteinase K (10 μg/mL, AM2546, Thermo Scientific, USA) for 20 minutes at 37 °C or, for GFP, with pepsin (Digest-All™ 00-3009, Invitrogen, USA) for 10 minutes at 37 °C. Subsequently, the slides were incubated with antibodies against periostin (1:1,000 diluted, ab14041, Abcam plc, UK), vWF (1:100 diluted, AB7356, EMD Millipore Co., USA), HLA (1:500 diluted, ab70328, Abcam plc, UK), and CEMP1 (1:1,000 diluted, sc-53947, Santa Cruz Biotechnology, USA) at 4 °C overnight. The specimens were sequentially incubated with secondary antibodies and streptavidin peroxidase. The results were visualized following staining with a diaminobenzidine (DAB) reagent kit (Invitrogen, USA). The sections were counterstained with Mayer's haematoxylin. And then, negative control staining was done without primary antibody. All specimens were observed using a stereomicroscope (MD5500D; Leica, camera: DFC495; Leica, Lens: HCX PL APO 409; Leica).

11. Statistical analysis

Statistical analysis was performed by one-way analysis of

variance (ANOVA) followed by Bonferroni's multiple comparison test using SPSS (ver.18) software for a comparison between the groups. $P < 0.05$ was used as the significance level.

III. Results

1. Characterization of hPDLSCs

Human PDLSCs from the extracted mandibular third molars were isolated and expanded. In order to characterize the hPDLSCs, flow cytometric analysis was performed using mesenchymal stem cell markers including CD13,CD34, CD90, and CD146.[22] Flow cytometric analysis showed that approximately 92.6% of the hPDLSCs expressed CD13, 94.52% expressed CD90, 80.71% expressed CD146, and 37.49% expressed CD34 (Fig. 5). CD34 is known as MSC-negative marker, which marks primitive endothelial cells and hematopoietic progenitors.[23]

Next, the multi-lineage differentiation capacity of hPDLSCs was evaluated *in vitro* with osteogenic, chondrogenic, and adipogenic medium. After 3 weeks of osteogenic and adipogenic induction, hPDLSCs formed extensive Alizarin red S-positive mineral deposits and Oil Red O-positive lipid droplets throughout the adherent layers. Furthermore, hPDLSCs also formed Alcian Blue-positive nodules after incubation in chondrogenic induction medium (Fig. 6).

2. Scanning Electron Microscopy (SEM) and

sample observation of bioprinted hPDLSCs

SEM showed that in the seeding groups (G1, G2), PDL cells had no direction and were not well organized, but in the printing groups (G3, G4), PDL cells were well aligned and had direction (Fig. 7). Bioink, a blend of hPDLSCs and 4 % collagen printed on a 3D printed titanium scaffold, was cultured until 21 days in gelation condition. The gelled bio-ink did not collapse but remained in its originally printed form in all groups till 21 days (Fig. 8).

3. Live/dead cell assay and proliferation assay

Live/dead cell assay showed that in cell seeding (G1, G2), the cell distribution was uneven and cell aggregation was observed. In the cell printing group (G3, G4), the cell distribution was homogeneous and confirmed to consist of single cells without cell aggregation (Fig. 9). As a result, we have confirmed that cell printing method is a more reliable method than seeding.

In the CCK-8 assay, shear stress occurred during printing and cell viability was lower than that of cell seeding group (G1, G2). However, cell printing group (G3, G4) proliferation has occurred well at day 7 (Fig. 10).

4. Gene expression of seeded and printed

hPDLSCs with real-time PCR

At Day 7 of culture, the expression of CEMP1 in the cell printing group (G3, G4) was significantly higher than in the cell seeding group (G1, G2) (Fig. 11). Col1 did not show any particular differences between both groups. The relative expression of ALP was more elevated in the seeding group (G1, G2) than printing group (G3, G4).

5. Animal experiments in athymic rat evaluating PDL regeneration *in vivo*

At 6 weeks after transplantation, the 3D printed titanium scaffolds were covered with fibrous connective tissue between the rat calvaria bone and 3D printed titanium scaffold in cell printing group (G3, G4) (Fig. 12). In decalicified tissue specimen, fibrous connective tissue was not observed in the seeding group (G1,G2) (Fig. 12). On the contrary fibrous connective tissue was apparent in the cell printing group (G3, G4) (Fig. 12). In undecalcified tissue specimen with H&E stain and basic fuchsin stain, new bone formation into porous scaffold was evident in seeding groups but in printing group, fibrous connective tissue was obvious between the rat calvaria bone and the scaffold (Fig. 13, 14). Immunohistochemical staining revealed that periostin, VWF, HLA, and CEMP1 were expressed

in the connective tissues produced in the cell printing group (G3, G4). But in negative control staining any of them were not expressed. According to this study, fgf−2 did not play a role in the regeneration of periodontal ligaments with bioprinting (Fig. 15).

IV. Discussion

The PDL is the fibrous connective tissue between the cementum, covering the root of the tooth, and the alveolar bone that forms the socket wall.[24] The PDL protects against infection and protect against bone resorption associated with mechanical stress, such as traumatic occlusal force and orthodontic tooth movement.[9, 10] The presence of a PDL can permit dynamic role even in a functionally ankyloses osseointegrated implant.[25] PDL-derived cells have stem cell-like characteristics and are regarded as versatile sources for periodontal reconstruction.[24] Many studies have demonstrated that periodontal ligament stem cells (PDLSCs) have ability of self-renewal and differentiation, clonogenicity, and capacity to produce connective tissue between cementum and bone.[13-16] Multi-lineage differentiation capacity of hPDLSCs *in vitro* with osteogenic, chondrogenic, and adipogenic medium was demonstrated in this study.

The problem that is expected when reconstructing jaws with 3D printed porous titanium is oral side exposure. For example, if the patient is to be reconstructed with a titanium 3D printing implant because of large segmental mandibular defect, the effectiveness of the specific mesh structure and surface treatment technology that promotes bone and adhesion to

enable immediate functioning should be confirmed. And the periodontal ligament regeneration technology at the implant interface near the oral mucosa so that the reconstructed implant can resist infection during oral exposure. To solve the problem, 3D printed hybrid artificial organ was fabricated by combining EBM technology and bioprinting of periodontal ligament in this study.

Osseointegrated dental implants have been regarded as being very reliable and having long-term predictability. However, host defense mechanisms against infection have been known to be impaired around a dental implant because of the lack of a periodontal ligament (PDL).[2, 8] To solve the problem, various bio-engineering methods for regenerating periodontal ligament around dental implant have been studied. Nyman *et al.* showed connective tissue attachment to teeth could be established using PDL cells in the monkey.[26] Several studies have proven that PDL tissue with cementum and fiber attachment to dental implant can be regenerated.[27-30] Lin *et al.* demonstrated three-dimensional biomatrix scaffold facilitated organized rat PDL regeneration at the interface between titanium implant and alveolar bone.[31] Recently, a method of regenerating periodontal ligament on the surface of titanium implant using PDL cell sheets has been widely used. PDL with cementum layer and

Sharpey' s fibers were regenerated using PDL cell sheets transplantation.[32] Another study showed that cell sheets from canine PDL stem cells with platelet-rich fibrin granules promotes periodontal regeneration in re-implanted avulsed tooth surface in a canine model.[33] Embryonic dental follicle tissue enclosed on the titanium implant, bio-hybrid implant was reported.[34] Another bio-hybrid implant encircled with PDL cell sheets trial, implanted in living bone tissue was tried[9].

No studies have attempted to regenerate periodontal ligament by printing periodontal ligament cells on the surface of titanium implants. Currently 3D cell-printing technique has been utilized as new biofabrication platform because of its ability to locate living cells in pre-defined spatial locations with scaffold and various growth factors.[17] Three dimensional (3D) bioprinting is the utilization of 3D printing and 3D printing-like techniques to combine cells, growth factors, and biomaterials to fabricate biomedical parts that maximally imitate natural tissue characteristics.[35] 3D bioprinted skin patch mixed with adipose-derived stem cells enhanced wound closure, re-epithelization, and neovascularization.[17] Implanted bioprinted neural stem cells in adult zebra fish accelerated repair of traumatic brain injury and restore of function.[36] In 2016 Kang *et al.* reported that implanted bioprinted various cell types including human

amniotic-derived stem cells, rabbit ear chondrocytes, and rabbit myoblasts produced newly formed vascularized bone tissue, cartilage, and muscle with physiologically relevant mechanical properties.[37]

Generally, 3D bioprinting utilizes the additive manufacturing which deposit materials known as bioinks to create tissue-like structures that are later used in medical and tissue engineering fields.[17] Bioprinting covers a broad range of biomaterials. In this study bio-ink was mixture of a commercial 4 % atelo-collagen (MS collagen, MSBIO Inc. Republic of Korea), recombinant human fibroblast growth factor basic-2 (FGF-2, ProSpec, Israel), and hPDLSCs with cell concentration in the bio-ink was $1x10^7$ cells/ml.

FGF-2 facilitates various cellular functions.[38] FGF2 promoted significant periodontal tissue repair with alveolar bone and cementum formation in beagle dog and non-human primates.[39-41] *In vitro* studies have shown that FGF-2 enhanced potent cellular proliferation and cell migration and regulated extracellular matrix formation by PDL cells.[42, 43] But according to this study, fgf-2 did not play a role in the regeneration of periodontal ligaments with bioprinting.

Various experiments were carried out to confirm that bio-

printing of periodontal ligaments is an effective method for regenerating periodontal ligament on 3D printing titanium. SEM showed that in the seeding groups (G1, G2), PDL cells had no direction and were not well organized, but in the printing groups (G3, G4), PDL cells were well aligned and had direction. Live/dead cell assay demonstrated that in cell seeding (G1, G2), the cell distribution was uneven and cell aggregation was observed. In the cell printing group (G3, G4), the cell distribution was homogeneous and confirmed to consist of single cells without cell aggregation (Fig. 9).

PDL-derived cells possess ability of periodontal regeneration including cementum formation.[24] CEMP-1 was known as one of the cementum marker genes found to be expressed in cementoblasts, PDL cells, and cells around vascular networks.[44, 45] At Day 7 of culture, the expression of CEMP1 in the cell printing group (G3, G4) was significantly higher than in the cell seeding group (G1, G2) (Fig. 11). This finding suggests that the printed PDL cells have the capacity for cementogenesis induction. At 6 weeks after transplantation, the 3D printed titanium scaffolds were covered with connective tissue between the rat calvaria and scaffold in cell printing group (G3, G4) (Fig. 12, 13, and 14). In decalcified tissue specimen, organized connective tissue was not observed in the seeding group (G1,

G2) (Fig.12). On the contrary well organized connective tissue was apparent in the cell printing group (G3, G4) (Fig. 12). In undecalcified tissue specimen with H&E stain and basic fuchsin stain, new bone formation into porous scaffold was evident in seeding groups but in printing group, well organized connective tissue was obvious between the rat calvaria and scaffold (Fig. 13, 14). Based on the results of this study, we conclude that PDL bioprinting technology is reliable method for regeneration of PDL on titanium 3D printed scaffold. Because the athymic rat model is versatile for validity assessment of human cell regeneration, we chose it to assess periodontal tissue regeneration induced by human PDL cell printing on 3D printed titanium scaffold. It was also required to confirm that newly formed PDL fibers are interconnected between the titanium and the bone, with a structure similar to that seen with natural periodontal tissue, and the rat calvaria is appropriate for the observation of PDL formation because of its profound blood supply.[8] Immunohistochemical staining revealed that periostin, VWF, HLA, and CEMP1 were expressed in the connective tissues produced in the cell printing group (G3, G4) (Fig. 15). Taken together, these results suggested that newly produced connective tissue between 3D printed implant and calvaria bone has PDL characteristics and originated from hPDLSCs.

3D printed hybrid artificial organ can also be applied to dental implants. 3D printed hybrid dental implant could establish physiological tooth functions, including the ability to react to mechanical stimulus and the ability to resist to infection. In order to apply bioprinting to a dental implant, techniques for bioprinting a spiral around the dental implant should be developed. In part I, SEM images demonstrate that 3D printed titanium samples' surface is entirely covered by globular micro-particles with different sizes arbitrarily disseminated on the surface. SEM is shown in Figure 11 (Part I). At 7 days, cellular extensions were observed between micro-particles that enhance strong anchoring of the hBMSCs. These findings implies that even without cementum on the surface of the implant, 3D printed titanium implants are likely to attach to the periodontal ligaments. Using 3D printed titanium as a scaffold for bioprinting other organs may help to organize the bioprinted cells.

V. Conclusion

Cell printing technology, rather than seeding periodontal ligament cells, has produced periostin positive-connective tissue interface between 3D printed titanium scaffold and the bone. Reconstruction with 3D printed hybrid artificial organ using bioprinting can be performed to prevent infection if the fibrous connective tissue, such as periodontal ligament is interposed between the titanium implant and the bone in the area close to oral mucosa. This study shows the potential for a next generation bio-implant coated with printed periodontal ligament resembling natural tooth using titanium 3D printing and PDL bioprinting for treating tooth loss.

References

1. Lee UL, Kwon JS, Woo SH, Choi YJ. Simultaneous Bimaxillary Surgery and Mandibular Reconstruction With a 3-Dimensional Printed Titanium Implant Fabricated by Electron Beam Melting: A Preliminary Mechanical Testing of the Printed Mandible. *J Oral Maxillofac Surg*. 2016; 74: 1501 e1501-1501 e1515.
2. Lee DJ, Lee JM, Kim EJ, Takata T, Abiko Y, Okano T *et al.* Bio-implant as a novel restoration for tooth loss. *Sci Rep*. 2017; 7: 7414.
3. Bertollo N, Da Assuncao R, Hancock NJ, Lau A, Walsh WR. Influence of electron beam melting manufactured implants on ingrowth and shear strength in an ovine model. *J Arthroplasty*. 2012; 27: 1429-1436.
4. Hrabe NW, Heinl P, Flinn B, Korner C, Bordia RK. Compression-compression fatigue of selective electron beam melted cellular titanium (Ti-6Al-4V). *J Biomed Mater Res B Appl Biomater*. 2011; 99: 313-320.
5. Joshi GV, Duan Y, Neidigh J, Koike M, Chahine G, Kovacevic R *et al.* Fatigue testing of electron beam-melted Ti-6Al-4V ELI alloy for dental implants. *J Biomed Mater Res B Appl Biomater*. 2013; 101: 124-130.

6. Wilde F, Hanken H, Probst F, Schramm A, Heiland M, Cornelius CP. Multicenter study on the use of patient-specific CAD/CAM reconstruction plates for mandibular reconstruction. *Int J Comput Assist Radiol Surg*. 2015; 10: 2035-2051.
7. Shan XF, Chen HM, Liang J, Huang JW, Cai ZG. Surgical Reconstruction of Maxillary and Mandibular Defects Using a Printed Titanium Mesh. *J Oral Maxillofac Surg*. 2015; 73: 1437 e1431-1439.
8. Washio K, Tsutsumi Y, Tsumanuma Y, Yano K, Srithanyarat SS, Takagi R *et al.* In Vivo Periodontium Formation Around Titanium Implants Using Periodontal Ligament Cell Sheet. *Tissue Eng Part A*. 2018; 24: 1273-1282.
9. Nakajima K, Oshima M, Yamamoto N, Tanaka C, Koitabashi R, Inoue T *et al.* Development of a Functional Biohybrid Implant Formed from Periodontal Tissue Utilizing Bioengineering Technology. *Tissue Eng Part A*. 2016; 22: 1108-1115.
10. Buser D, Warrer K, Karring T. Formation of a periodontal ligament around titanium implants. *J Periodontol*. 1990; 61: 597-601.
11. Bengel FM, Ueberfuhr P, Schiepel N, Nekolla SG,

Reichart B, Schwaiger M. Effect of sympathetic reinnervation on cardiac performance after heart transplantation. *N Engl J Med*. 2001; 345: 731-738.

12. Huch K, Muller KA, Sturmer T, Brenner H, Puhl W, Gunther KP. Sports activities 5 years after total knee or hip arthroplasty: the Ulm Osteoarthritis Study. *Ann Rheum Dis*. 2005; 64: 1715-1720.

13. Chen SC, Marino V, Gronthos S, Bartold PM. Location of putative stem cells in human periodontal ligament. *Journal of periodontal research*. 2006; 41: 547-553.

14. Gronthos S, Mrozik K, Shi S, Bartold PM. Ovine periodontal ligament stem cells: isolation, characterization, and differentiation potential. *Calcif Tissue Int*. 2006; 79: 310-317.

15. Ivanovski S, Gronthos S, Shi S, Bartold PM. Stem cells in the periodontal ligament. *Oral diseases*. 2006; 12: 358-363.

16. Kaneda T, Miyauchi M, Takekoshi T, Kitagawa S, Kitagawa M, Shiba H *et al.* Characteristics of periodontal ligament subpopulations obtained by sequential enzymatic digestion of rat molar periodontal ligament. *Bone*. 2006; 38: 420-426.

17. Kim BS, Kwon YW, Kong JS, Park GT, Gao G, Han W *et*

al. 3D cell printing of *in vitro* stabilized skin model and in vivo pre-vascularized skin patch using tissue-specific extracellular matrix bioink: A step towards advanced skin tissue engineering. *Biomaterials*. 2018; 168: 38-53.

18. Jin B, Choung PH. Recombinant Human Plasminogen Activator Inhibitor-1 Accelerates Odontoblastic Differentiation of Human Stem Cells from Apical Papilla. *Tissue Eng Part A*. 2016; 22: 721-732.

19. Park JY, Choi JC, Shim JH, Lee JS, Park H, Kim SW *et al.* A comparative study on collagen type I and hyaluronic acid dependent cell behavior for osteochondral tissue bioprinting. *Biofabrication*. 2014; 6: 035004.

20. Shim JH, Kim JY, Park M, Park J, Cho DW. Development of a hybrid scaffold with synthetic biomaterials and hydrogel using solid freeform fabrication technology. *Biofabrication*. 2011; 3: 034102.

21. Shim JH, Jang KM, Hahn SK, Park JY, Jung H, Oh K *et al.* Three-dimensional bioprinting of multilayered constructs containing human mesenchymal stromal cells for osteochondral tissue regeneration in the rabbit knee joint. *Biofabrication*. 2016; 8: 014102.

22. Parolini O, Alviano F, Bagnara GP, Bilic G, Buhring HJ, Evangelista M *et al.* Concise review: isolation and

characterization of cells from human term placenta: outcome of the first international Workshop on Placenta Derived Stem Cells. *Stem Cells*. 2008; 26: 300-311.

23. Dominici M, Le Blanc K, Mueller I, Slaper-Cortenbach I, Marini F, Krause D *et al.* Minimal criteria for defining multipotent mesenchymal stromal cells. The International Society for Cellular Therapy position statement. *Cytotherapy*. 2006; 8: 315-317.

24. Seo BM, Miura M, Gronthos S, Bartold PM, Batouli S, Brahim J *et al.* Investigation of multipotent postnatal stem cells from human periodontal ligament. *Lancet (London, England)*. 2004; 364: 149-155.

25. Giannobile WV. Getting to the root of dental implant tissue engineering. *Journal of clinical periodontology*. 2010; 37: 747-749.

26. Nyman S, Gottlow J, Karring T, Lindhe J. The regenerative potential of the periodontal ligament. An experimental study in the monkey. *Journal of clinical periodontology*. 1982; 9: 257-265.

27. Buser D, Warrer K, Karring T, Stich H. Titanium implants with a true periodontal ligament: an alternative to osseointegrated implants? *Int J Oral Maxillofac Implants*. 1990; 5: 113-116.

28. Choi BH. Periodontal ligament formation around titanium implants using cultured periodontal ligament cells: a pilot study. *Int J Oral Maxillofac Implants*. 2000; 15: 193-196.

29. Takata T, Katauchi K, Miyauchi M, Ogawa I, Akagawa Y, Nikai H. Periodontal tissue regeneration on the surface of synthetic hydroxyapatite implanted into root surface. *J Periodontol*. 1995; 66: 125-130.

30. Warrer K, Karring T, Gotfredsen K. Periodontal ligament formation around different types of dental titanium implants. I. The self-tapping screw type implant system. *J Periodontol*. 1993; 64: 29-34.

31. Lin Y, Gallucci GO, Buser D, Bosshardt D, Belser UC, Yelick PC. Bioengineered periodontal tissue formed on titanium dental implants. *Journal of dental research*. 2011; 90: 251-256.

32. Flores MG, Yashiro R, Washio K, Yamato M, Okano T, Ishikawa I. Periodontal ligament cell sheet promotes periodontal regeneration in athymic rats. *Journal of clinical periodontology*. 2008; 35: 1066-1072.

33. Zhao YH, Zhang M, Liu NX, Lv X, Zhang J, Chen FM *et al.* The combined use of cell sheet fragments of periodontal ligament stem cells and platelet-rich fibrin granules for avulsed tooth reimplantation. *Biomaterials*. 2013; 34:

5506-5520.

34. Oshima M, Inoue K, Nakajima K, Tachikawa T, Yamazaki H, Isobe T *et al.* Functional tooth restoration by next-generation bio-hybrid implant as a bio-hybrid artificial organ replacement therapy. *Sci Rep*. 2014; 4: 6044.

35. Singh D, Thomas D. Advances in medical polymer technology towards the panacea of complex 3D tissue and organ manufacture. *American journal of surgery*. 2018.

36. Hsieh FY, Lin HH, Hsu SH. 3D bioprinting of neural stem cell-laden thermoresponsive biodegradable polyurethane hydrogel and potential in central nervous system repair. *Biomaterials*. 2015; 71: 48-57.

37. Kang HW, Lee SJ, Ko IK, Kengla C, Yoo JJ, Atala A. A 3D bioprinting system to produce human-scale tissue constructs with structural integrity. *Nature biotechnology*. 2016; 34: 312-319.

38. Folkman J, Shing Y. Angiogenesis. *The Journal of biological chemistry*. 1992; 267: 10931-10934.

39. Murakami S, Takayama S, Ikezawa K, Shimabukuro Y, Kitamura M, Nozaki T *et al.* Regeneration of periodontal tissues by basic fibroblast growth factor. *Journal of periodontal research*. 1999; 34: 425-430.

40. Murakami S, Takayama S, Kitamura M, Shimabukuro Y, Yanagi K, Ikezawa K *et al.* Recombinant human basic fibroblast growth factor (bFGF) stimulates periodontal regeneration in class II furcation defects created in beagle dogs. *Journal of periodontal research*. 2003; 38: 97-103.

41. Takayama S, Murakami S, Shimabukuro Y, Kitamura M, Okada H. Periodontal regeneration by FGF-2 (bFGF) in primate models. *Journal of dental research*. 2001; 80: 2075-2079.

42. Shimabukuro Y, Terashima H, Takedachi M, Maeda K, Nakamura T, Sawada K *et al.* Fibroblast growth factor-2 stimulates directed migration of periodontal ligament cells via PI3K/AKT signaling and CD44/hyaluronan interaction. *Journal of cellular physiology*. 2011; 226: 809-821.

43. Takayama S, Murakami S, Miki Y, Ikezawa K, Tasaka S, Terashima A *et al.* Effects of basic fibroblast growth factor on human periodontal ligament cells. *Journal of periodontal research*. 1997; 32: 667-675.

44. Hoz L, Romo E, Zeichner-David M, Sanz M, Nunez J, Gaitan L *et al.* Cementum protein 1 (CEMP1) induces differentiation by human periodontal ligament cells under

three-dimensional culture conditions. *Cell biology international*. 2012; 36: 129-136.

45. Alvarez-Perez MA, Narayanan S, Zeichner-David M, Rodriguez Carmona B, Arzate H. Molecular cloning, expression and immunolocalization of a novel human cementum-derived protein (CP-23). *Bone*. 2006; 38: 409-419.

Figure Legends and Figures

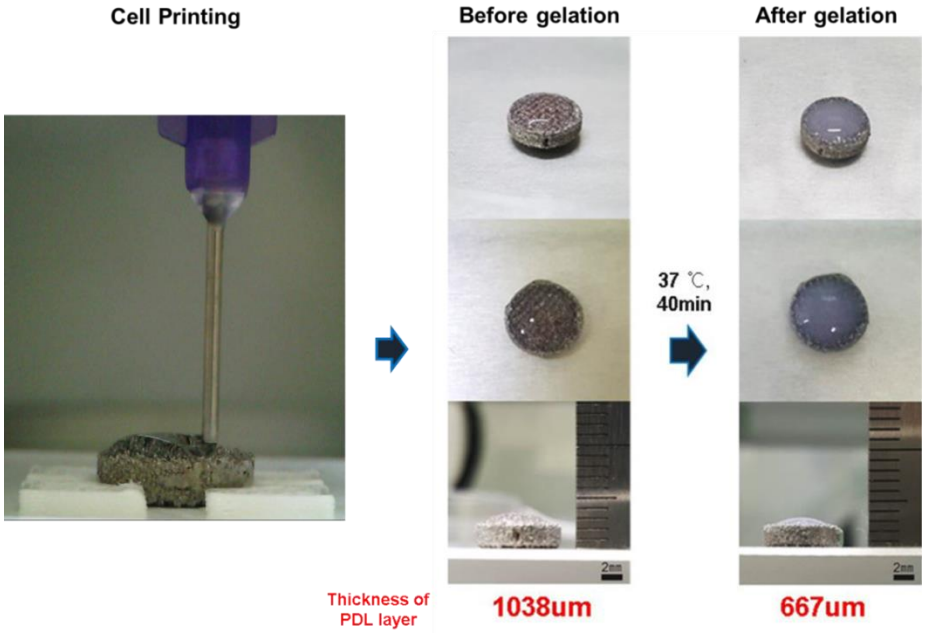

Figure 1. Bioprinting process for periodontal ligament regeneration

A commercial 4 % atelo-collagen (MS collagen, MSBIO Inc. Republic of Korea) and recombinant human fibroblast growth factor basic-2 (FGF-2, ProSpec, Israel) were prepared. After that, periodontal ligament stem cells were seeded on the printed bioink without cells (group 1: titanium scaffold/collagen/cell seeding, group 2: titanium scaffold/collagen+FGF-2/cell seeding). In the cell printing group, the bioinks with cells (group 3: titanium scaffold/collagen/cell printing, group 4: titanium scaffold/collagen+FGF-2/cell printing) were printed one layer on a 3D printed titanium scaffold surface and stored for 30 min at 37℃ for gelation.

Figure 2. Bioprinter.

For precise cell printing experiment, bioprinter (3DX Printer, T&R Biofab Co., Ltd., Republic of Korea) was utilized.

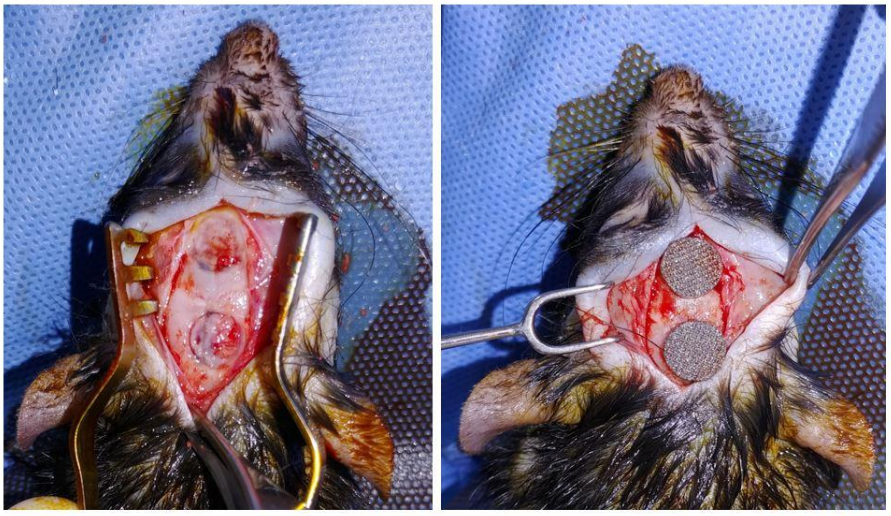

Figure 3. Animal experiments in athymic rat

Using 8 mm trephine bur, 2 circular shaped bone ditches were made not penetrated into dura with a diameter of 8 mm on

rat’ s calvaria. And using round bur, a bony pit with a depth of 1.5 mm inside the circle was made on calvaria. 4 groups of samples were transplanted after 2 days of incubation with bioprinted PDL cell layer in contact with the calvarial bone.

Figure 4. Harvested samples

Six weeks after transplantation, the rats were euthanized, and the calvaria with implanted specimens were harvested.

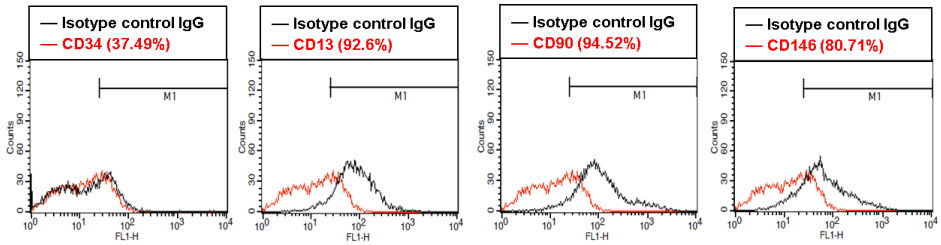

Figure 5. Fluorescence-activated cell sorting analysis of hPDLSCs using mesenchymal stem cell markers, including CD13, CD34, CD90, and CD146

Flow cytometric analysis showed that approximately 92.6% of the hPDLSCs expressed CD13, 94.52% expressed CD90, 80.71% expressed CD146, and 37.49% expressed CD34.

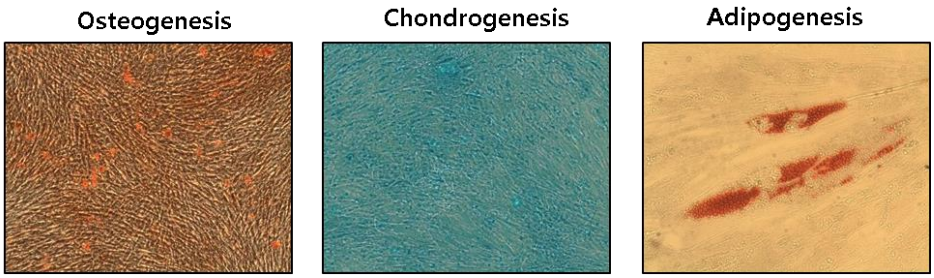

Figure 6. Multilineage differentiation capacity of hPDLSC *in vitro* with osteogenic, chondrogenic, and adipogenic medium After 3 weeks of osteogenic and chondrogenic induction, hPDLSCs formed extensive Alizarin red S-positive mineral deposits and Oil Red O-positive lipid droplets throughout the adherent layers. Furthermore, hPDLSCs also formed Alcian Blue-positive nodules after incubation in chondrogenic induction medium.

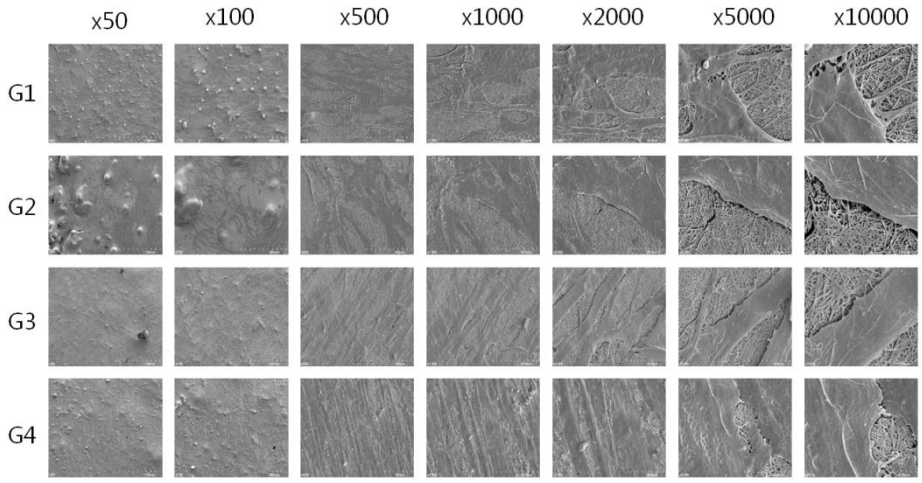

Figure 7. Scanning Electron Microscopy

SEM showed that in the seeding groups (G1, G2), PDL cells had no direction and were not well organized, but in the printing groups (G3, G4), PDL cells were well aligned and had direction.

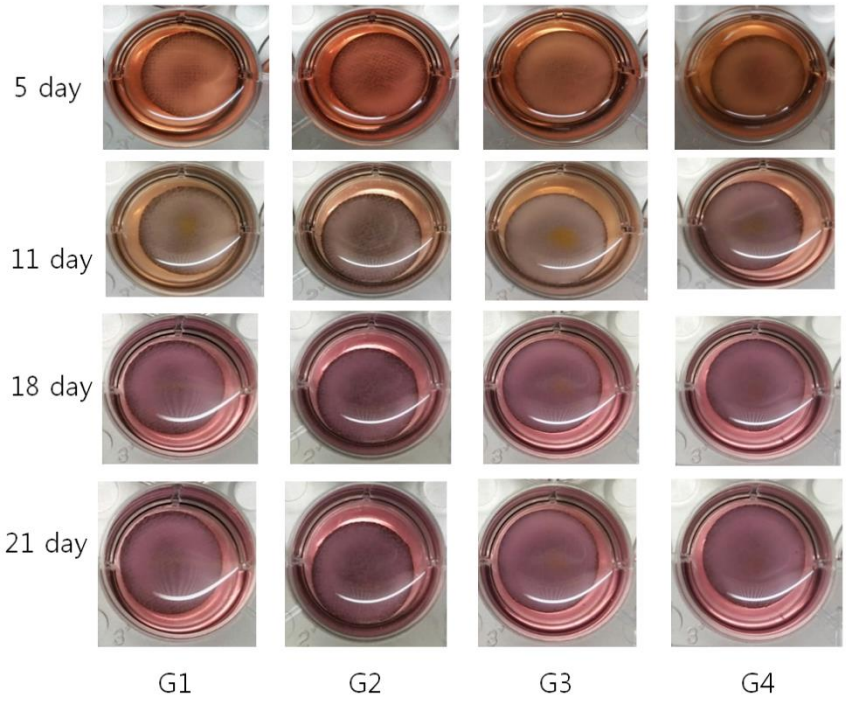

Figure 8. The gelled bioink did not collapse but remained in its originally printed forms in all groups till 21 days.

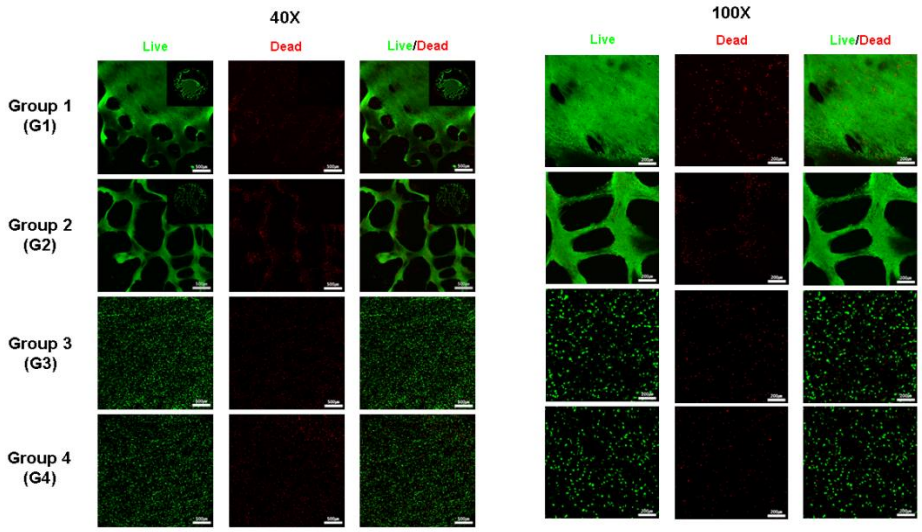

Figure 9. Live/dead cell assay

Live/dead cell assay showed that in cell seeding (G1 & G2), the cell distribution was uneven and cell aggregation was observed. In the cell printing group (G3 & G4), the cell distribution was homogeneous and confirmed to consist of single cells without cell aggregation. * $p<0.05$

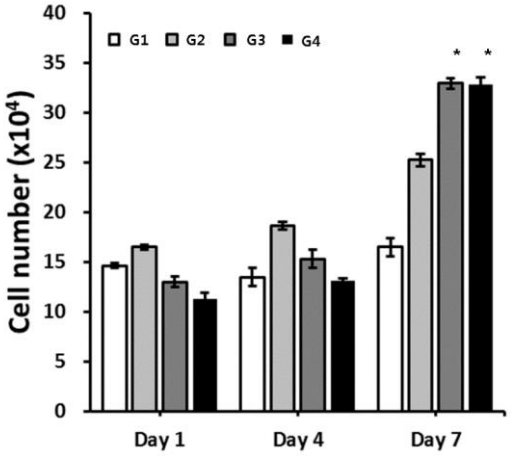

Figure 10. Proliferation assay

In the CCK-8 assay, shear stress occurred during printing and cell viability was lower than that of cell seeding group (G1, G2). Proliferation of cell printing group (G3 & G4) has occurred well at day 7. * $p<0.05$

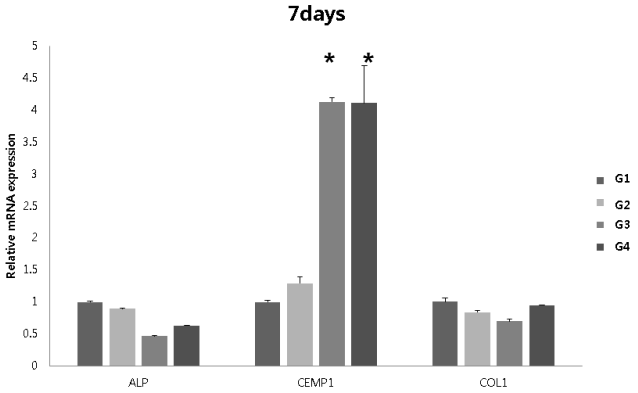

Figure 11. Real-time PCR

At Day 7 of culture, the expression of CEMP1 in the cell printing group (G3, G4) was significantly higher than in the cell seeding group (G1, G2) with real-time PCR.

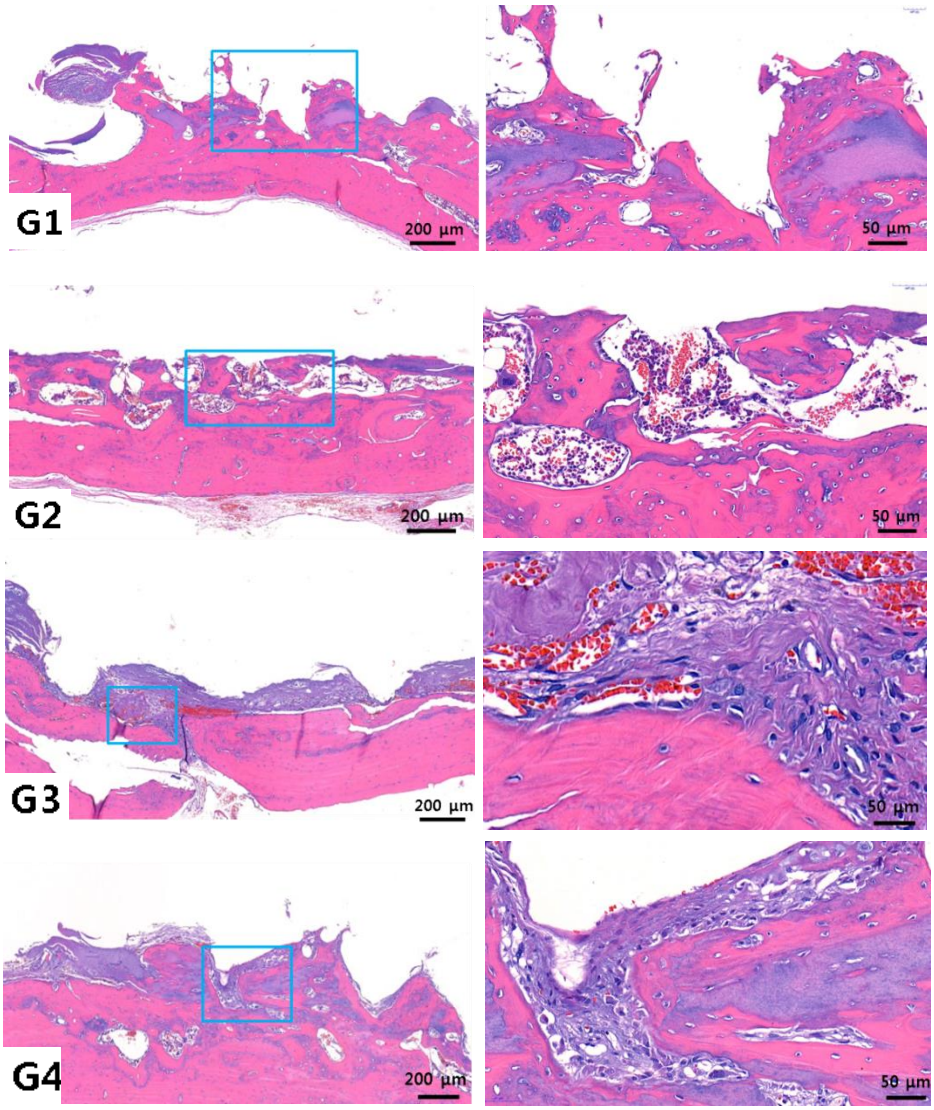

Figure 12. Decalcified cross-section of the samples (G1-G4), H&E stain

In decalicified tissue specimen, fibrous connective tissue was not observed in the seeding group (G1,G2). On the contrary well organized fibrous connective tissue was apparent in the cell printing group (G3, G4).

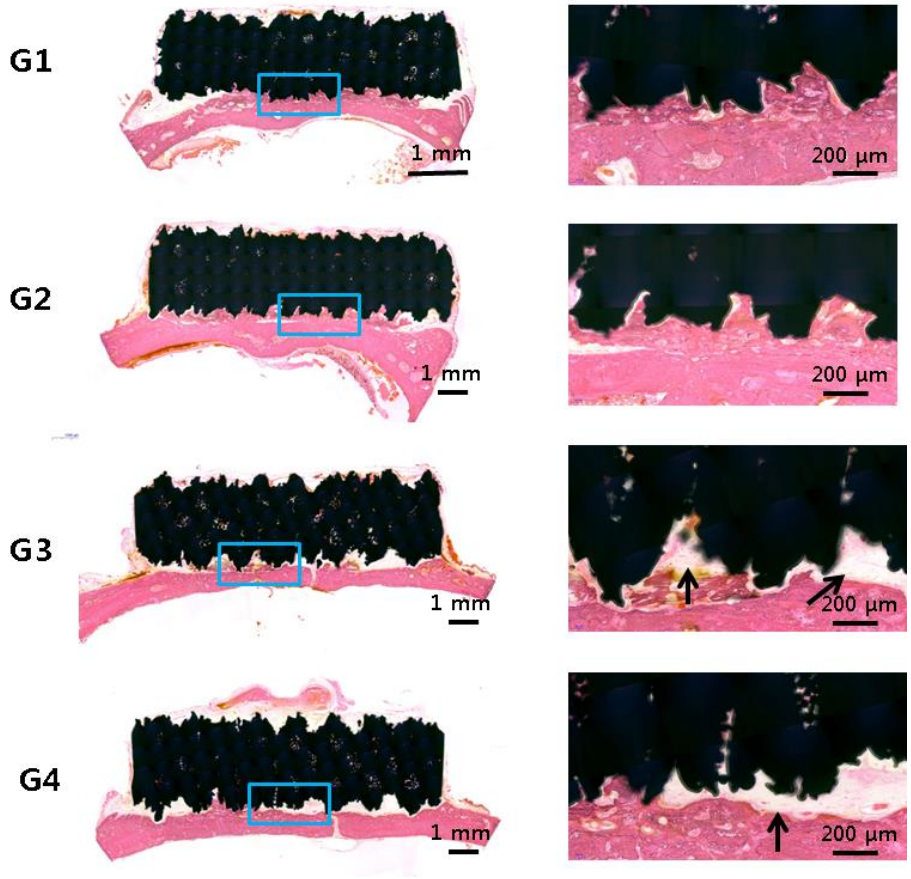

Figure 13. Undecalcified cross-section of the samples (G1-G4), H&E stain

In undecalcified tissue specimen with H&E stain, new bone formation into porous scaffold was evident in seeding groups (G1,G2), but in printing group (G3, G4), well organized fibrous connective tissue (arrow) was obvious between the rat calvaria and scaffold.

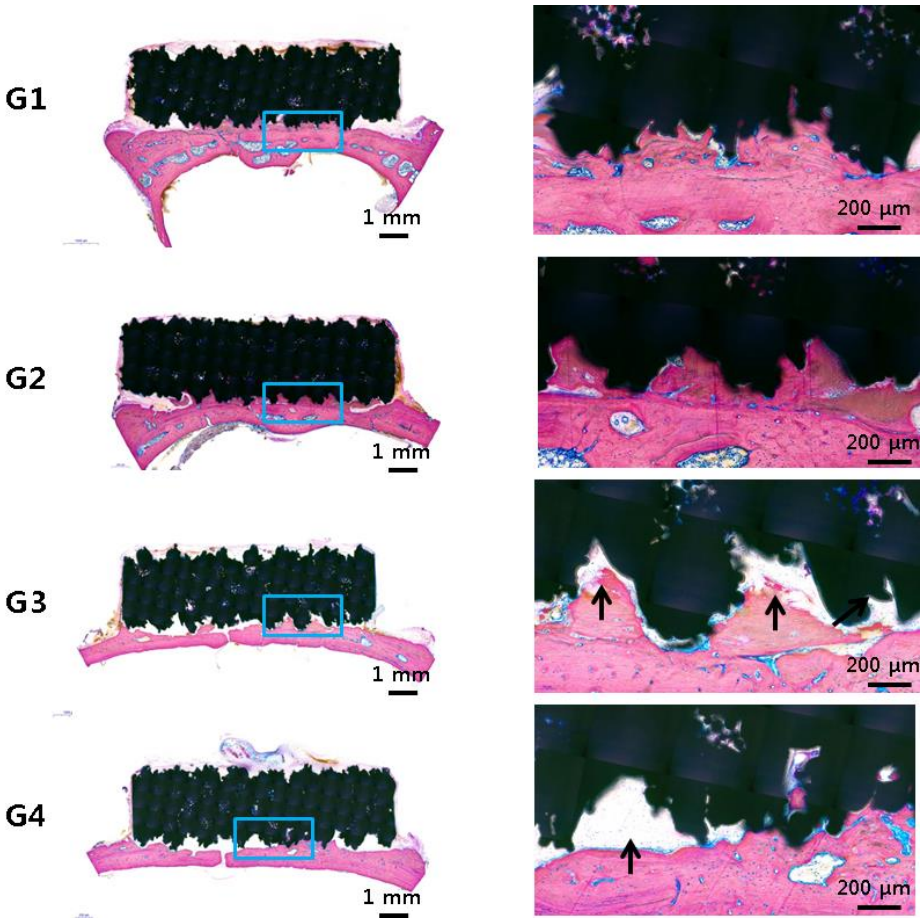

Figure 14. Decalcified cross-section of the samples (G1-G4), basic fuchsin stain

In undecalcified tissue specimen with basic fuchsin stain, new bone formation into porous scaffold was evident in seeding groups (G1, G2) but in printing group (G3, G4), well organized fibrous connective tissue (arrow) was observed between the rat calvaria and scaffold.

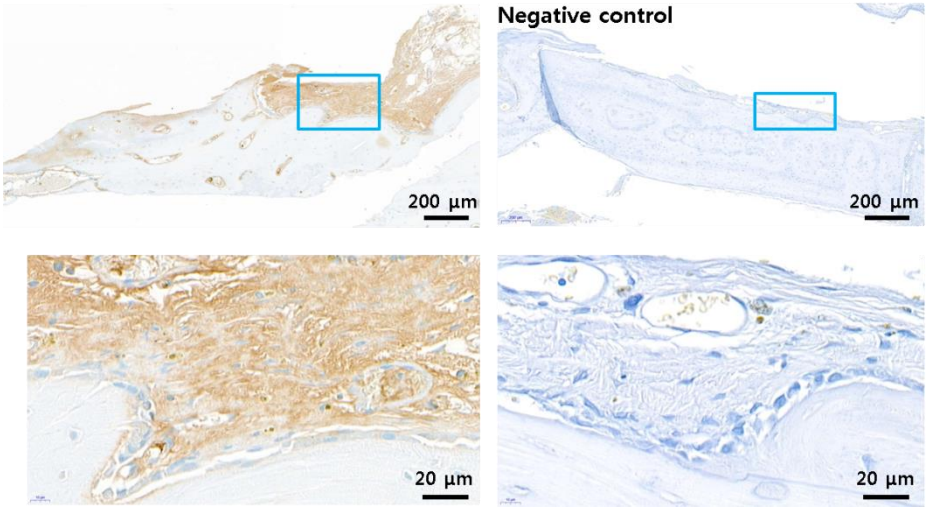

A. Immunohistochemistry of HLA, G3

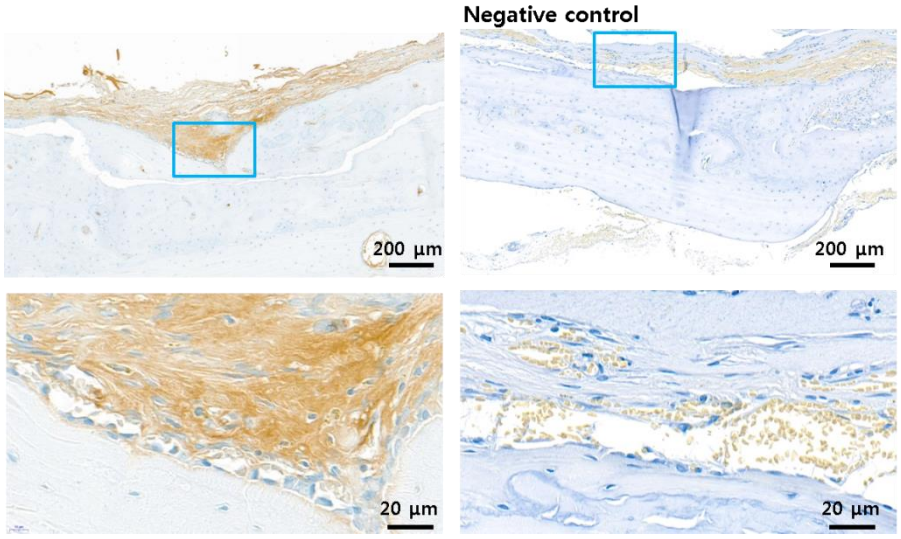

B. Immunohistochemistry of HLA, G4

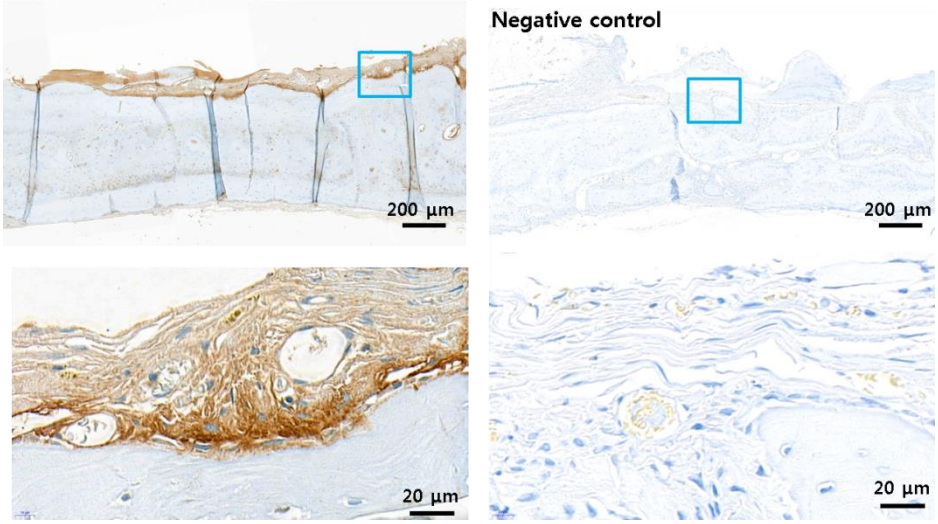

C. Immunohistochemistry of periostin, G3

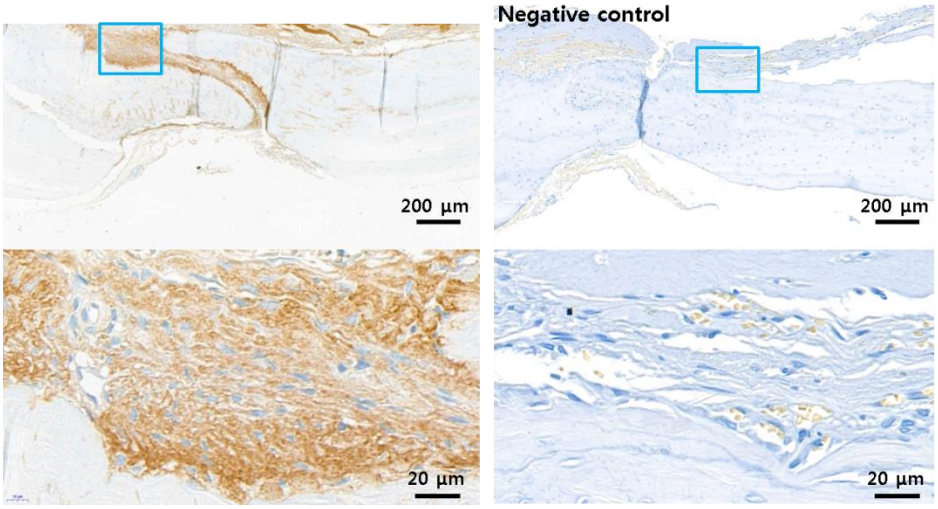

D. Immunohistochemistry of periostin, G4

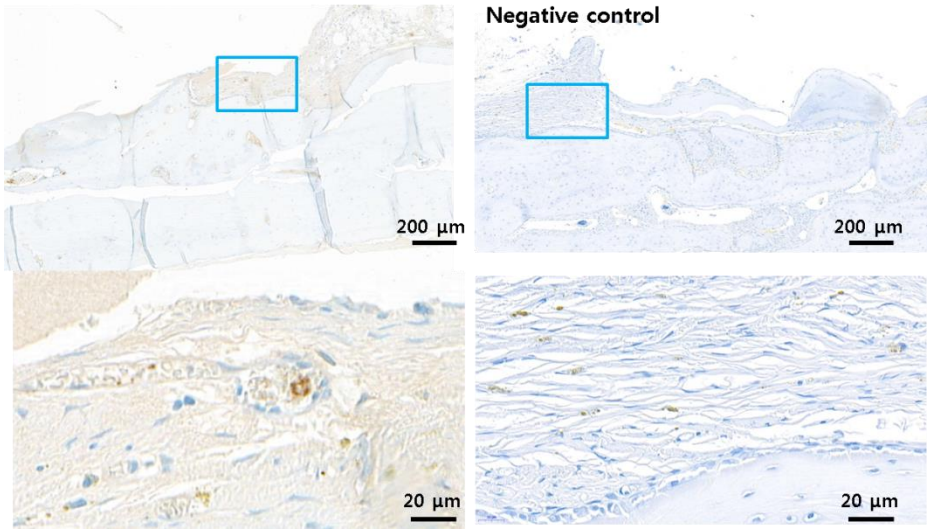

E. Immunohistochemistry of vWF, G3

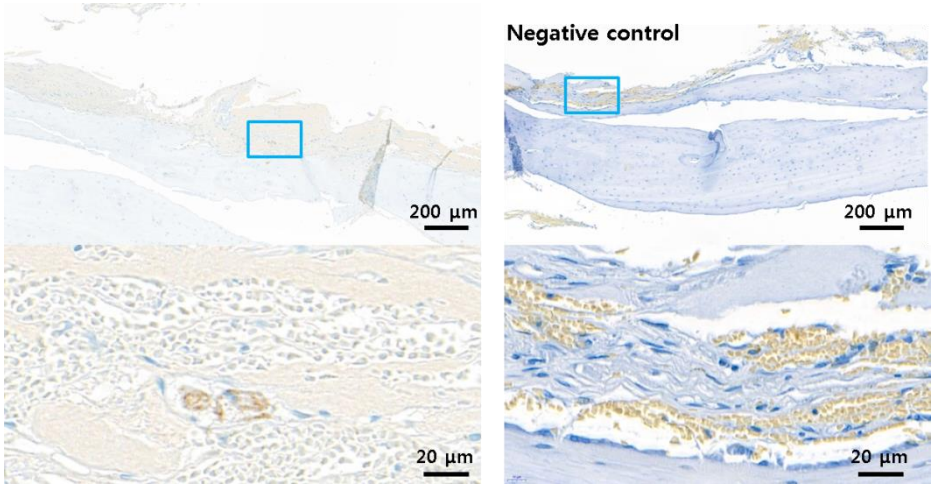

F. Immunohistochemistry of vWF, G4

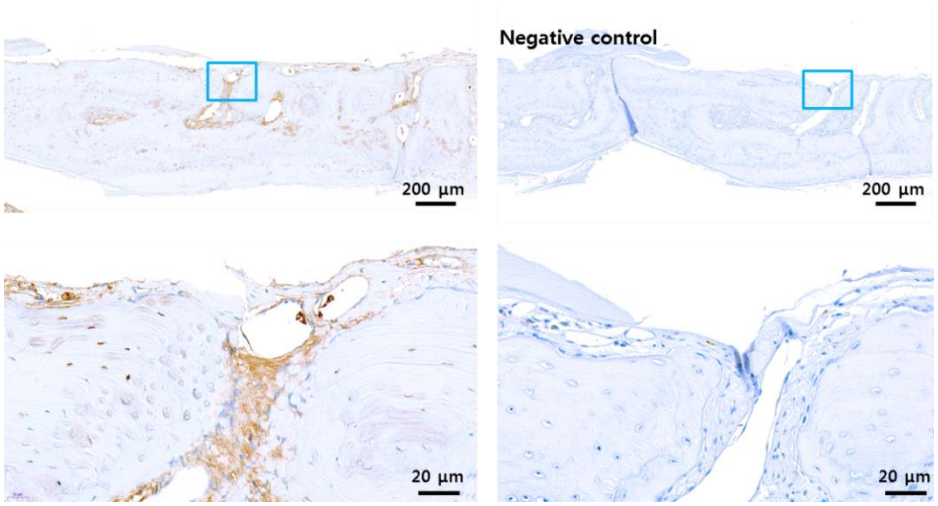

G. Immunohistochemistry of CEMP1, G3

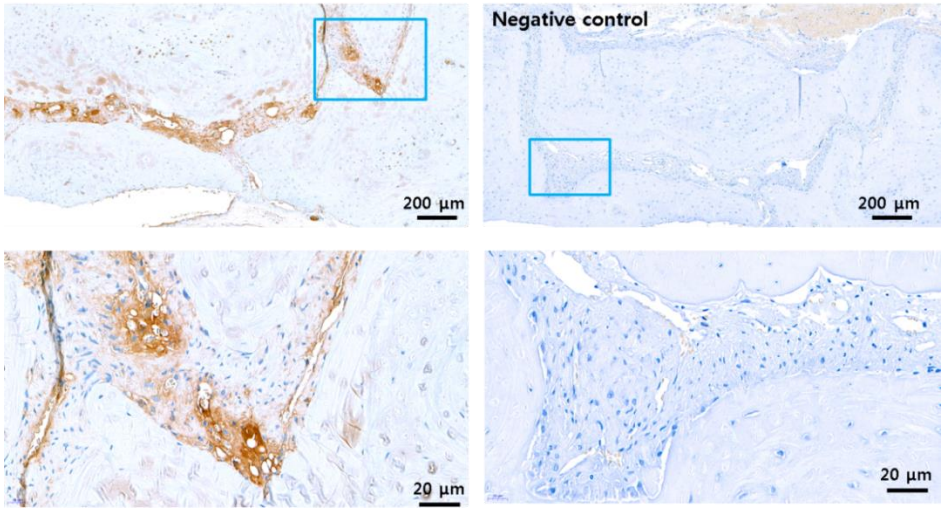

H. Immunohistochemistry of CEMP1, G4

Figure 15A–H. Immunohistochemical staining

Immunohistochemical staining revealed that Periostin, vWF, HLA, and CEMP 1 were expressed in the tissues produced in

the cell printing group (G3, G4). But in negative control staining any of them were not expressed.

Tables

Target cDNA	Forward Primer sequence (5’ −3’)	Reverse Primer sequence (5’ −3’)
ALP	TAAGGACATCGCCTACCAGCTC	TCTTCCAGGTGTCAACGAGGT
COL1	AACATGGAGACTGGTGAGACCT	CGCCATACTCGAACTGGAATC
CEMP1	TCAAGGCAGAGGTGGGTATC	GGAAATGTCTCCAGGTCCAA
GAPDH	CTTTGGTATCGTGGAAGGACTC	GTAGAGGCAGGGATGATGTTCT

Table 1. Primer sequences

국문초록

악안면 재건을 위한 3D 프린팅 매식체

Part I. 다양한 티타늄 3D 프린팅 구조체의 골융합

Part II. 티타늄 3D 프린팅 다공성 스캐폴드에서 바이오프린팅 기술을 적용한 치주인대의 재생

구강악안면외과학 전공 이 의 룡 (지도교수 : 정필훈)

1. 목 적

악안면 영역은 생존에 필요한 음식 저작의 기능을 담당할 뿐 아니라, 언어 구사 및 외모와 같은 사회적 기능을 담당하는 중요한 부위이다. 외상, 선천성 기형, 양성 및 악성 종양 등의 원인으로 결손이 발생하였을 때 기능적, 심미적인 재건수술이 필요하다. 악안면 재건을 위해서 신체의 타 부위로부터 이식을 하는 방법이 성공적으로 사용되고 있지만 수술이 어렵고 공여부합병증, 및 비심미적 결과 등 다양한 문제가 있다.

이를 극복하기 위하여 환자 맞춤형 티타늄 3D 프린팅 보형물을 사용하여 악안면 영역을 재건하는 방법이 유럽과 미국을 중심으로 이루어지고 있으며 국내에서도 환자 맞춤형 3D 프린팅 티타늄

보형물이 식약처 허가를 득하였고 점점 많은 술자에 의하여 악골 재건에 사용되고 있다. 하지만 티타늄 3D 프린팅 보형물의 생체적합성 및 골유착을 증진시킬 수 있는 다공성 구조, 표면처리 등의 연구가 드문 상태이다. 그리고 골유착 치과 임플란트는 현재 널리 쓰이고 있으니 생체 치아를 모방하지 못하고 있다. 즉 주변에 치주인대가 없어서 감염에 대한 숙주 방어 메커니즘이 없고 미세쿠션기능이 없어서 임플란트 주위골이 쉽게 손상되는 것으로 알려져 있다. 이 문제를 해결하기 위해 본 연구에서는 티타늄 3D 프린팅 기술과 치주인대 바이오프린팅 기술을 융합하여 기존의 티타늄 픽스쳐가 구현할 수 없는 치주인대로 구성된 연조직 계면을 티타늄 구조체 주위에 형성한 3D 프린팅 하이브리드 임플란트를 개발 하였다.

본 연구의 목적은 티타늄 3D 프린팅 다공성 구조, 양극산화법, 및 세포 프린팅 기술을 융합하여 악안면 영역 재건을 위한 골유착능이 우수하고 생체적합적인 3D 프린팅 구조체를 개발하고 실제 치아를 모사하는 바이오 임플란트를 개발하는 것이다.

2. 방 법

사람 제3대구치 발치 시 채취된 조직에서 치조골 줄기세포 및 치주인대 줄기세포를 분리 및 배양하였고 줄기세포 특성을 분석하였다. 생체적합성 연구를 위하여 티타늄 강재를 절삭가공한 샘플 (STi), 다공성 구조가 없는 3D 프린팅 솔리드 티타늄 (3DPSTi), 및 3D 프린팅 다공성 티타늄 (3DPMTi) 샘플을 제작

하였다. 각 샘플의 절반을 양극산화해서 총 6개 그룹 (STi, ASTi, 3DPSTi, A3DPSTi, 3DPMTi, A3DPMTi)으로 실험을 진행하였다. 다양한 샘플 위에 치조골 줄기세포를 배양하고 세포 부착능 분석, 세포 증식 분석, 주사형 전자현미경 관찰 및, 실시간 중합효소연쇄반응을 시행하여 각 샘플의 생체적합성을 분석하였다.

뼈융합력 연구를 위하여 솔리드 구조와 다양한 다공성 구조로 티타늄 프린팅 하여 2.5*6.0 mm의 임플란트 기둥을 얻은 후 절반을 양극산화 하였다. 가토의 대퇴골에 다양한 다공성 구조의 임플란트를 식립하고 6주후 대퇴골을 채취하고 푸쉬-아웃 테스트를 시행하여 골유착능을 비교하고 마이크로씨티 촬영 및 조직시편을 제작하였다.

원판모양의 도드씬 구조의 티타늄 3D 프린팅 다공성 스캐폴드에 치주인대 줄기세포를 피펫팅하여 파종한 그룹 (G1, G2)과 세포 프린팅한 그룹 (G3, G4), 그리고 FGF-2를 혼합한 그룹 (G2, G4)과 그렇지 않은 그룹 (G1, G3)으로 나누어 실험하였다. 각 샘플의 라이브 및 데드 분석, 증식분석, 및 실시간 중합효소연쇄반응을 시행 하였다. 치주인대가 세포 프린팅 된 3D 프린팅 티타늄 스캐폴드를 누드랫의 두개골에 치주인대가 프린팅된 부분이 두개골표면에 닿도록 이식하고 6주후에 스캐폴드와 두개골을 함께 채취하였다. 조직을 마이크로씨티를 촬영하고 탈회시편, 비탈회시편을 제작 하였으며 면역조직화학 염색을 시행하였다.

3. 결 과

유세포 분석결과 치조골 줄기세포 및 치주인대 줄기세포에서 모두 줄기세포 표지자인 CD13, CD90, CD146이 발현 되었으며 골, 연골, 지방으로 분화될 능력이 있는 줄기세포의 특징을 가지고 있음을 확인하였다. 양극산화 샘플에서 세포부착능이 양극산화를 하지 않은 샘플보다 우수하였다. 3D 프린팅 솔리드 샘플 보다는 3D 프린팅 다공성 샘플에서 세포부착능이 우수했으며 절삭 샘플 보다는 3D 프린팅 샘플에서 세포 부착능이 우수하였다. 주사형 전자현미경 관찰 결과 양극산화 샘플에서 세포가 더욱 견고하게 부착 되어 있음이 관찰 되었다. 모든 샘플에서 양극산화를 한 경우에 세포 증식력이 더 높았으며, 절삭 샘플 보다는 3D 프린팅 샘플에서 세포 증식력이 높았다. 골 형성 유전자 발현 분석에서 가장 두드러진 특징은 양극산화 처리 된 샘플에서 OPG의 발현이 높고 RANKL의 발현이 낮다는 점이다.

가토의 대퇴골에서 진행된 푸쉬-아웃 테스트에 의하면 절삭 샘플보다 3D 프린팅 샘플이 골유착이 훨씬 우수하였다. 양극산화는 3D 프린팅 다공성 구조체에서 골유착을 증진시켰다. 특히 3D 프린팅 솔리드 구조체는 다공성 구조체 보다 골융합이 우수하였다. 마이크로씨티 소견 상 3D 프린팅 샘플에서 모두 골유착이 도출되었으며 3D 프린팅 샘플의 경우 양극산화를 한 샘플과 하지 않은 샘플 사이에 큰 차이가 없었으므로 이는 굳이 양극삭회를 할 필요 없이 사용 가능함을 시사한다. 조직학적분석에 따르면 임플란트 주변 피질골 영역에서 양극산화처리하지 않은 절삭샘플을

제외한 모든 샘플에서 임플란트가 골유착 되어있었다.

4%의 콜라젠을 치주인대 줄기세포에 혼합하여 바이오 잉크를 제조하는 것이 3%나 5% 콜라젠을 혼합하는 것보다 세포 프린팅을 위해 적절하였다. 피펫팅을 이용한 세포파종 그룹에서는 세포 분포가 불균일하게 나타났으며 세포 뭉침 현상이 관찰 되었다. 세포 프린팅 그룹에서는 세포 분포가 균일하였으며, 세포 뭉침 현상 없이 단일세포로 구성되어 있었다. 겔화 된 바이오 잉크는 붕괴되지 않고 21 일까지 모든 그룹에서 원래 프린팅 된 형태로 유지되었다. CCK-8 분석결과 증식 7일째 세포 프린팅 그룹 (G3, G4)의 증식은 세포 파종 그룹 (G1, G2)보다 높았다. 배양 7일째, 세포 프린팅 그룹에서의 CEMP1의 발현은 세포 파종 그룹보다 높게 발현 되었다.

이식 6주 후 두개골 채취시 3D 프린팅 티타늄 스캐폴드는 모두 두개골에 견고하게 부착되어 있었다. 조직소견상 세포 파종 그룹에서는 스캐폴드와 두개골이 골유착이 되어 있음이 관찰 되었지만 세포 프린팅 그룹에서는 스캐폴드와 두개골 사이에 섬유성 결합조직이 생성되어 있음을 관찰하였다. 면역조직화학 염색 결과 세포 프린팅 그룹에서 생성된 조직에 Periostin, vWF, HLA, 그리고 CEMP1이 발현되었다.

4. 결론

티타늄 3D 프린팅 구조체는 기존의 절삭가공으로 제조된 티타늄 구조체 보다 생체친화성 및 골융합이 우수하였다. 양극산화는 3D

프린팅 다공성 구조체에서 골유착을 증진시켰으나 3D 프린팅 솔리드 구조체에서는 영향력이 없었다. 3D 프린팅 솔리드 구조체는 다공성 구조체 보다 골융합이 우수하였다. 따라서 티타늄 3D 프린팅 솔리드 구조체는 임상적으로 악골 재건에 성공적으로 사용될 수 있을 것이다. 그리고 치주인대 세포를 파종하는 방법보다 세포 프린팅 하는 것이 치주인대가 재생될 수 있는 가능성을 높혔다. 치주인대 세포를 티타늄 3D 프린팅 스캐폴드 표면에 세포 프린팅 하여 생체 치아를 모사하는 3D 프린팅 하이브리드 임플란트가 개발되었다. 본 연구를 통하여 치추인대가 없이 골유착 되는 기존 임플란트의 한계를 극복할 수 있는 단초를 마련 하였다.

주요어 : 줄기세포, 티타늄 3D 프린팅, 양극산화, 다공성 구조, 바이오프린팅, 생체적합성, 푸쉬-아웃 테스트, 골유착, 3D 프린팅 하이브리드 임플란트

학번 : 2009-31124